Aryl Hydrocarbon Receptor-Mediated Induction of EBV Reactivation as a Risk Factor for Sjögren's Syndrome

Hiroko Inoue,* Kenji Mishima,*,[1] Sachi Yamamoto-Yoshida,* Ryoko Ushikoshi-Nakayama,* Yoichi Nakagawa,[†] Ken Yamamoto,[‡] Kofuchi Ryo,* Fumio Ide,* and Ichiro Saito*

The aryl hydrocarbon receptor (AhR) is a ligand-activated transcription factor that mediates a variety of biological effects by binding to environmental pollutants, including 2,3,7,8-tetrachlorodibenzo-*p*-dioxin (TCDD or dioxin). Although numerous animal studies have demonstrated the harmful effects of dioxins, it remains controversial whether dioxins pose a risk to human health. Enhanced lytic replication of EBV is a risk factor for the development of autoimmune diseases and cancers. This study evaluated the possibility that ligand-activated AhR reactivates EBV. EBV reactivation and AhR transactivation were evaluated with luciferase assays. Saliva samples were collected from 19 patients with primary Sjögren's syndrome (SS). Control saliva samples were obtained from 10 healthy individuals and nine patients with severe dry mouth. TCDD enhanced BZLF1 transcription, which mediates the switch from the latent to the lytic form of EBV infection in EBV-positive B cell lines and in a salivary gland epithelial cell line. Moreover, TCDD-induced increases in BZLF1 mRNA and EBV genomic DNA levels were confirmed in the B cell lines. Saliva from SS patients activated the transcription of both CYP1A1 and BZLF1. Additionally, there was a positive correlation between CYP1A1 and BZLF1 promoter activities. AhR ligands elicited the reactivation of EBV in activated B cells and salivary epithelial cells, and these ligands are involved in SS. Our findings reveal novel aspects of the biological effects of dioxin and the AhR-dependent pathogenesis of autoimmune diseases. *The Journal of Immunology*, **2012, 188: 4654–4662.**

Halogenated aromatic hydrocarbons, including 2,3,7,8-tetrachlorodibenzo-*p*-dioxin (TCDD or dioxin), are chemical carcinogens that are widely distributed in the environment, and these chemicals are persistent environmental contaminants. Human exposure to mixtures of halogenated aromatic hydrocarbons and polynuclear aromatic hydrocarbons occurs mainly through diet; thus, exposure is universal and can accumulate throughout a lifetime. Most of the harmful effects of dioxins are thought to be mediated by the aryl hydrocarbon receptor (AhR) (1–3). The binding of ligands to the AhR triggers its translocation into the nucleus, where the AhR forms a heterodimer with the AhR nuclear translocator (Arnt). The AhR/Arnt heterodimer binds to specific xenobiotic response elements located in the promoter and enhancer regions of target genes, thus regulating the transcription of these genes.

Dioxins directly induce the replication of the influenza virus (4), human CMV (5), and HIV type 1 (6) in vitro. Moreover, viral titers in the salivary glands of rats infected with CMV are elevated by dioxin in vivo (7). Although numerous animal studies have demonstrated the harmful effects of dioxins, the dioxin-related risks to human health remain controversial.

EBV is a ubiquitous herpes virus that infects >90% of the world's population. Infection is usually asymptomatic and associated with lifelong persistence of the virus in resting recirculating memory B cells (8). The induction of lytic replication results in new viral infection and EBV-associated cellular transformation, and this induction may be a risk factor for both malignant transformation and the development of autoimmune diseases. The pathogenesis of many autoimmune diseases, including multiple sclerosis, systemic lupus erythematosus, Sjögren's syndrome (SS), and rheumatoid arthritis, is not fully understood. Both genetic predisposition and environmental factors, including EBV infection, contribute to the development and/or promotion of these diseases (9).

During viral replication, the EBV BZLF1 is the first gene to be transcribed. Its gene product Zta (also called ZEBRA, EB1, and Z) is considered both necessary and sufficient to induce the EBV lytic cycle (10, 11). The regulatory elements within the BZLF1 promoter (Zp) are divided into three groups: positive elements (ZI, ZII, and ZIIIA), negative elements (H1, ZIIR, ZIV, and ZV), and autoreactivation elements (ZIIIA and ZIIIB) (12). The region from −221 to +12 bp, which carries the ZI, ZII, ZIII, and ZV motifs, may be necessary for maintaining basal activity and transcriptional activation by lytic cycle-inducing agents (13). Conversely, the distal region from −554 to -221 bp contains repressive elements (14). In latently infected B cells, BZLF1 expression leading to viral replication is induced by various reagents, including phorbol ester (15), anti-Ig Abs (16), and butyrate (17). However, the physiological

*Department of Pathology, Tsurumi University School of Dental Medicine, Kanagawa 230-8501, Japan; [†]Department of Oral and Maxillofacial Surgery, Tsurumi University School of Dental Medicine, Kanagawa 230-8501, Japan; and [‡]Department of Geriatric Dentistry, Tsurumi University School of Dental Medicine, Kanagawa 230-8501, Japan

[1]Current address: Department of Oral Pathology and Diagnosis, School of Dentistry, Showa University, Tokyo, Japan.

Received for publication May 27, 2011. Accepted for publication February 27, 2012.

This work was supported by a grant-in-aid for scientific research from the Japan Society for the Promotion of Science (to H.I.) and the Science Research Promotion Fund from the Promotion and Mutual Aid Corporation for Private Schools of Japan Act (to I.S.). This work was also supported in part by a grant from the Strategic Research Foundation Grant-aided Project for Private Universities from the Ministry of Education, Culture, Sports, Science and Technology-Japan.

Address correspondence and reprint requests to Prof. Ichiro Saito, Department of Pathology, Tsurumi University School of Dental Medicine, 2-1-3 Tsurumi, Tsurumi-ku, Kanagawa 230-8501, Japan. E-mail address: saito-i@tsurumi-u.ac.jp

Abbreviations used in this article: AhR, aryl hydrocarbon receptor; Arnt, aryl hydrocarbon receptor nuclear translocator; CALUX, chemically activated luciferase gene expression; DM, dry mouth; HA, hemagglutinin; NML, normal healthy individual; SS, Sjögren's syndrome; TCDD, 2,3,7,8-tetrachlorodibenzo-*p*-dioxin; TPA, 12-*O*-tetradecanoyl-phorbol-13-acetate; XBP-1, X-box binding protein-1; Zp, BZLF1 promoter; Zta, EBV BZLF1 gene.

www.jimmunol.org/cgi/doi/10.4049/jimmunol.1101575

stimulant that controls the initiation of viral replication and the switch from latency in vivo is unknown.

B cells are a major component of humoral immunity and are a sensitive immune target of TCDD (18). Resting human B cells are also the main sites of primary EBV infection in vivo. In healthy individuals, EBV persists in the memory B cells of the mucosal lymphoid tissue in the Waldeyer's ring (tonsils/adenoids) and in the peripheral blood for the duration of the individual's lifespan. EBV-infected memory B cells from this reservoir can be induced to enter the lytic phase of infection, which is accompanied by the differentiation of the B cells into plasma cells (19).

In this study, we demonstrate that BZLF1 is a novel target gene of dioxin-activated AhR. Infectious EBV is present in both the saliva of SS patients (20–22) and culture supernatants of B cell lines established from SS patients (23). Mariette et al. (24) previously used in situ hybridization to detect EBV DNA in a substantial proportion of lymphoid cells and epithelial cells in salivary glands from patients with SS. In our study, saliva from SS patients transactivated both BZLF1 and CYP1A1, which are target genes of AhR. Taken together, these findings demonstrate that the AhR ligands in SS saliva may be involved in EBV reactivation. Although dioxins are known to modulate the immune system, resulting in the development of autoimmune diseases, our study suggests a new role for dioxins as a pathogenetic factor for autoimmune disease via EBV reactivation.

Materials and Methods

Cell culture

The EBV-positive B cell lines B95-8 (an EBV-transformed marmoset B cell line) and P3HR1 (a Burkitt's lymphoma cell line) were maintained in RPMI 1640 supplemented with penicillin (100 IU/ml), streptomycin (100 mg/ml), and 10% FCS. These cell lines promptly and synchronously activated latent EBV genomes after 12-*O*-tetradecanoyl-phorbol-13-acetate (TPA) stimulation. The cells were suspended in fresh medium to produce a final concentration of 1×10^6 cells/ml and were cultured for the indicated time in the presence or absence of TPA. The salivary adenocarcinoma cell line HSY (25) (provided by Dr. M. Sato, Tokushima University) was cultured in MEM containing penicillin (100 IU/ml), streptomycin (100 μg/ml), and 10% FCS.

Plasmids

The promoter region (−552 to +13) of BZLF1 was amplified by PCR and cloned into pGL3 basic luciferase vector (Promega) using the primers pZp+13Hind (5′-CGAAGCTTGCCGGCAAGGTGCAATGTTT-3′) and pZp−551Xho (5′-AGCTCGAGGGATCCCTAACGCCAG-3′). The following combinations of enzymes were used to construct the pZp221-Luc and pZp130-Luc plasmids: XhoI-SphI for Zp221 and XhoI-NsiI for Zp130. Constructs pZp552Δ130, MI, MII, and MIII were synthesized from pZp552-Luc by temperature cycling using the primers and PfuTurbo DNA polymerase. These constructed pZp plasmids are shown in Fig. 1. Reporter DNA construct containing the human CYP1A1 promoter was generated by inserting a 1.9-kb CYP1A1 promoter PCR fragment into the pGL3 basic luciferase vector.

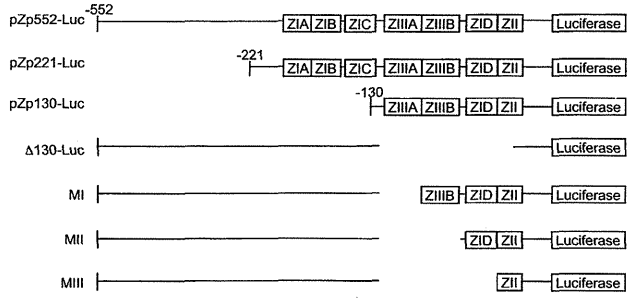

FIGURE 1. Schematic description of the relevant plasmids used in transfection experiments to analyze the transcriptional *cis*-elements.

To construct the expression vectors pCI-AhR-hemagglutinin (HA) and pCI-Arnt-HA, the AhR and Arnt cDNAs were amplified by RT-PCR and subcloned into pCI-neo (Promega), and an HA tag was fused to the C-terminal end of the gene. The RT-PCR primers used were as follows: AhR, 5′-CTCGAGACCATGAACAGCAGC-3′ and 5′-ACGCGTCAGGAATCCACTG-3′; and Arnt, 5′-CGCTCGAGGCCATGGCGGCGACT-3′ and 5′-GTACGCGTTTCTGAAAAGGGGGGA-3′. To construct Ad-AhR-HA and Ad-Arnt-HA, HA-tagged cDNAs were excised from pCI-AhR-HA and pCI-Arnt-HA and inserted into the cosmid pAxCAwt (TaKaRa, Shiga, Japan). Viral titers were measured in a limiting dilution bioassay using HEK293 cells.

Reporter assay

Cells were seeded in 12- or 24-well plates at a density of 10^6 cells per well and grown to subconfluence. HSY cells were seeded in 12-well plates 24 h prior to transfection. Transient transfection experiments were performed using Lipofectamine 2000 (Invitrogen) according to the manufacturer's protocol. Cells were cotransfected with the pZp552-Luc, pZp221-Luc, pZp130-Luc, or CYP1A1-Luc reporters using 1 ng *Renilla* luciferase reporter (pRL-TK) driven by the HSV thymidine kinase (HSV-tk) promoter as an internal control and the pCI-AhR, pCI-Arnt, or pCI-Zta plasmid using Lipofectamine 2000. After 4 h, transfected cells were treated with either TCDD or a vehicle control (DMSO) for 48 h. Final DNA concentrations were adjusted using empty expression vectors to ensure that equal amounts of DNA were used in each well. Cells were harvested and lysed in a passive lysis buffer (Promega). Lysates were sequentially assayed for firefly and *Renilla* luciferase activity in a luminometer using the dual luciferase reporter assay system (Promega) and an ARVO MX multilabel counter (PerkinElmer). The results are presented in terms of relative luciferase activity, which represents the ratio of stimulated activity to nonstimulated activity in each experiment. All transfection experiments were performed in triplicate.

Quantitative PCR

Total RNA (2 μg) was used for cDNA synthesis with the SuperScript III first-strand synthesis system (Invitrogen). Quantitative PCR was performed using the SYBR Premix Ex Taq II kit (TaKaRa) and analyzed on a StepOnePlus instrument (Applied Biosystems). The PCR primers used were as follows: BZ1, 5′- TTCCACAGCCTGCACCAGTG-3′; BZ2, 5′-GGCAGCAGCCACCTCACGGT-3′; BRLF1 up, 5′-CATCACTATAGGGCACGCGA-3′; BRLF1 down, 5′-TAATGGCCACGCTCAACATC-3′; BALF5 up, 5′-CGGAAGCCCTCTGGACTTC-3′; and BALF5 down, 5′-CCCTGTTTATCCGATGGAATG -3′. The latter two primers recognize the EBV viral DNA BALF5 gene that encodes the viral DNA polymerase. Briefly, each 20-μl reaction sample contained 2 μl cDNA or genomic DNA, 10 μl SYBR Premix Ex Taq II (TaKaRa), 0.4 μl ROX reference dye, 0.8 μl each primer at 10 μM, and 6 μl double-distilled H_2O. Each experiment was run in triplicate. The PCR reaction was conducted as follows: 95°C for 30 s, followed by 40 cycles of 95°C for 3 s and 60°C for 30 s.

EMSA

HSY cells were infected with Ad-AhR and Ad-Arnt and then stimulated with TCDD for 2 h. Cell lysates were extracted from Ad-AhR– and Ad-Arnt–infected HSY cells using the CelLytic M cell lysis reagent (Sigma-Aldrich) and stored at −80°C until the assay was performed. EMSA was carried out with the LightShift chemiluminescent EMSA kit (Pierce Chemical). Oligonucleotide probe for Zp130 was biotinylated using the biotin 3′ end-labeling kit (Pierce Chemical). Briefly, cell lysates were incubated with 20 fmol biotin-labeled oligonucleotide for 20 min at room temperature in a binding buffer (10 mM Tris, 1 mM EDTA, 1 mM DTT, 100 mM KCl, and 10% [v/v] glycerol) and 1 μg nonspecific inhibitor Poly (deoxyinosinic-deoxycytidylic) in a final volume of 20 μl and incubated for 20 min at 25°C, followed by nondenaturing gel electrophoresis using 0.5× TAE as the running buffer. After electrophoresis, the biotinylated probes were transferred to a Hybond N+ membrane (GE Healthcare) followed by cross-linking with UV light. The biotinylated DNA was imaged using a VersaDoc 5000 (Bio-Rad). The specificity of AhR DNA binding was determined by competition reactions in which a 200-fold molar excess (4 pmol) of unlabeled oligonucleotide was added to the binding reaction.

Saliva samples

All SS patients were evaluated at the outpatient clinic of the Tsurumi University School of Dental Medicine (Yokohama, Japan) and diagnosed based on criteria proposed by the Japan Ministry of Health, Labor, and Welfare (Table I). Saliva samples were collected from 19 patients with SS (mean age, 61.9 y) at the initial medical examination, prior to the ad-

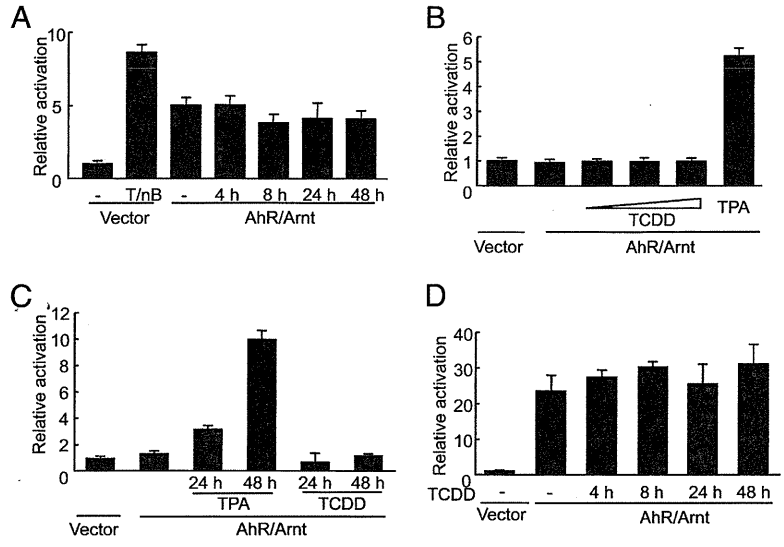

FIGURE 2. TCDD did not activate Zp or CYP1A1 transcription in unstimulated B cell lines. (**A**) pZp552-Luc was transiently cotransfected with human AhR and Arnt into P3HR1 cells cultured for the indicated times in the presence of 100 nM TCDD, TPA/n-butylate, TPA, and *n*-butylate. (**B** and **C**) Human AhR and Arnt were cotransfected into the Zp552-B95-8 stable cell line. Zp activities were measured after 24 and/or 48 h stimulation with either TPA (100 ng/ml) or TCDD [1–100 nM (B) or 100 nM (C)]. (**D**) CYP1A1-Luc was transiently cotransfected with human AhR and Arnt into P3HR1 cells and cultured for the indicated times in the presence of 100 nM TCDD. Values represent means ± SD derived from the normalized data, with transfections performed in triplicate in each experiment. Data were averaged over at least three experiments.

ministration of any medication. Control saliva samples were obtained from 10 age-matched normal healthy individuals (NML) (mean age, 63.7 y) and 9 patients with severe dry mouth (DM; mean age, 58.1 y). Informed consent was obtained from all patients. The average stimulated and unstimulated saliva flow rates in both SS and DM individuals were <5 ml/10 min and <0.5 ml/15 min, respectively. Samples were centrifuged at 12,000 × *g* for 45 min and filtered through a 0.22-μm filter to remove cells, viruses, and particulate debris. Aliquots of the samples were then stored at −80°C.

Ethics

Informed consent was obtained from all patients, and the Ethical Committee of Tsurumi University approved this study.

Results

TCDD does not change the EBV infectious status in B cell lines

To test the effect of TCDD on EBV reactivation in B lymphocytes, we used the EBV-infected B cell lines B95-8 and P3HR1, in which the EBV lytic cycle can be induced by TPA stimulation in vitro. Because BZLF1 expression following Zp reactivation is sufficient for this switch (10), we initially conducted a Zp assay to confirm EBV reactivation in B cells. pZp552-Luc, indicated in Fig. 1, was transiently transfected into P3HR1, and TCDD had no effect on Zp552 activation, even in the presence of AhR and Arnt expression (Fig. 2A). We also tested the stably transfected cell line Zp552-B95-8. Zp552 activation was strongly enhanced in Zp552-B95-8 cells following TPA stimulation, but the cells did not respond to TCDD in the presence of AhR and Arnt (Fig. 2B, 2C). Moreover, the promoter activity of CYP1A1, a target gene of AhR, was unchanged following TCDD stimulation, even in the presence of AhR and Arnt (Fig. 2D). Although B cells have previously demonstrated an inappropriate activation response to TCDD (26), our results show that TCDD stimulation alone is not sufficient for AhR activation or for BZLF1 and CYP1A1 transcription in P3HR1 and B95-8 cells.

TCDD induces EBV reactivation in TPA-activated B cell lines

Several studies have demonstrated that activated B cells are more sensitive to TCDD than are nonactivated cells (27–29). TPA-activated splenocytes show increased AhR expression and enhanced dioxin response element binding to AhR in the presence of TCDD (28). Thus, we studied the effect of TCDD on B cells under moderate activation by TPA. P3HR1 and B95-8 cells were stimulated with a low concentration of TPA (1 ng/ml) prior to incubation with TCDD. Simultaneous TPA and TCDD treatment enhanced the transactivation of pZp552 compared with treatment with TPA alone (Fig. 3). TPA combined with *n*-butylate stimulated Zp552, and the greatest activity was detected after 48 h incubation (Fig. 2C). In contrast, under moderate TPA stimulation, TCDD increased Zp552 activity after as little as 6 h stimulation, and the maximum activity was observed after 24 h (Fig. 3). The increased expression of BZLF1 mRNA was confirmed by RT-PCR (Fig. 4A) and real-time PCR (Fig. 4B), and significant expression was detected after 24 h combined TCDD/TPA treatment (Fig. 4A, 4B). EBV genomic DNA was amplified by PCR using primers for the BALF5 gene, and the levels of this DNA were increased in B95-8 and P3HR1 cells following treatment with TCDD combined with TPA (Fig. 4C). Real-time PCR revealed significant EBV replication after 24 or 48 h treatment in P3HR1 and B95-8 cells, respectively (Fig. 4D). At the point when virus replication was confirmed, the mRNA expression of an alternative virus gene, BRLF1, was also increased in these cells (Fig. 4E, 4F). These results suggest that the activation of B cells is required for TCDD

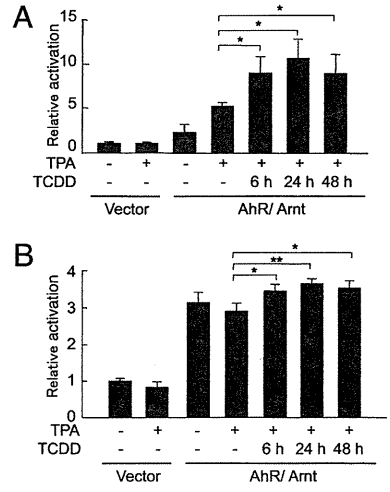

FIGURE 3. Transactivation of Zp by TCDD in TPA-activated B cell lines. Human AhR and Arnt were cotransfected into P3HR-1 (**A**) and B95-8 cells (**B**). Zp activities were measured after 6, 24, and 48 h stimulation with TCDD (100 nM) in the presence of TPA (1 ng/ml). Values represent means ± SD derived from normalized data, with transfections performed in triplicate in each experiment. Data were averaged over at least three experiments. Statistical analysis was performed using a one-way ANOVA. $*p < 0.05$, $**p < 0.005$.

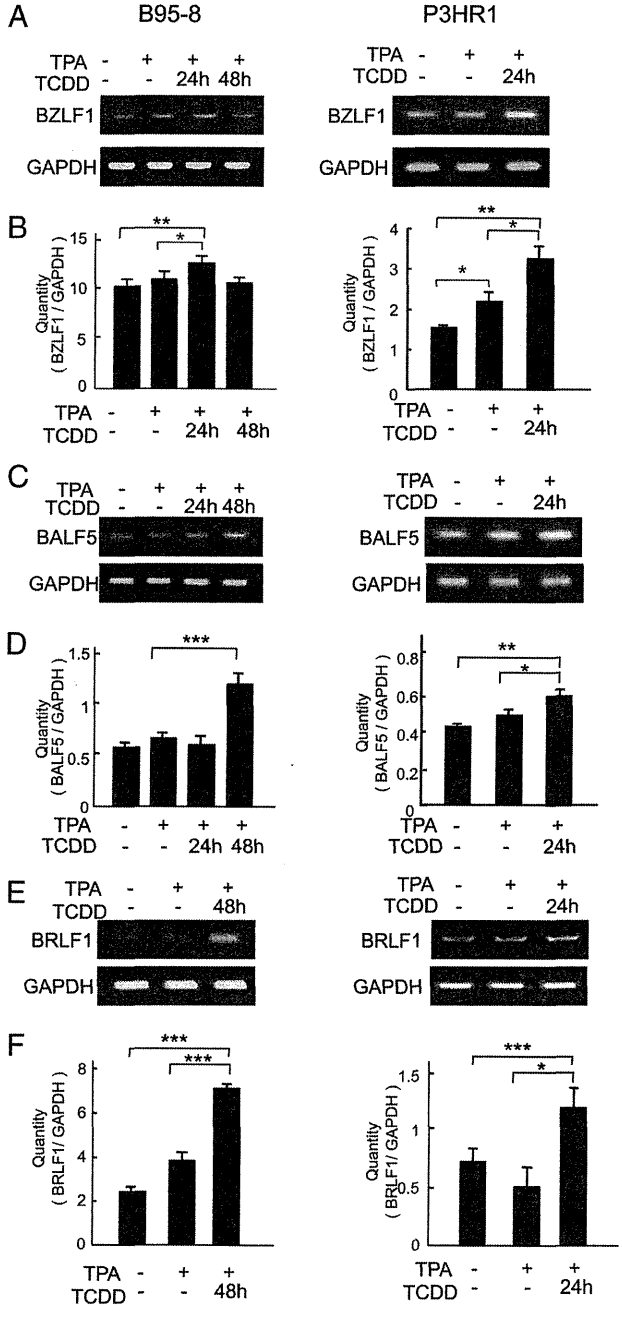

FIGURE 4. EBV gene expression and replication by TCDD in TPA-activated B cell lines. mRNA and genomic DNA were obtained from B95-8 (*left panels*) and P3HR1 (*right panels*) cells stimulated with TCDD (100 nM) in the presence of TPA (0.01 ng/ml). RT-PCR (**A, E**) and real-time RT-PCR (**B, F**) analysis of BZLF1 (A, B) and BRLF1 (E, F) transcripts. PCR (**C**) and real-time PCR (**D**) analyses were conducted for BALF5 to represent EBV genomic DNA. Real-time PCR results are presented relative to GAPDH mRNA expression (B, F) or genomic DNA (D). Values represent means ± SD derived from normalized data, with transfections performed in triplicate in each experiment. Data were averaged over at least three experiments. Statistical analysis was performed using a one-way ANOVA. $*p < 0.05$, $**p < 0.005$, $***p < 0.0005$.

to reactivate EBV and emphasize that Zp activity reflects BZLF1 mRNA expression and EBV replication.

TCDD induces Zp activation in salivary gland epithelial cells

EBV replication only occurs in a small percentage of B cells (30), and the levels of virus released from B cells alone differs considerably from the actual virus levels in the saliva (31). Thus, EBV reactivation in B cells is thought to be only the initial event in the spread of virus particles in vivo. The actual physiological site of virus production is thought to be the epithelial cells of the nasopharynx and parotid glands (31–34). The calculated potential virus production from these cells is sufficient to account for the observed levels of shedding in saliva (31). Thus, we tested Zp activation in the salivary epithelial cell line HSY.

HSY cells were cotransfected with pZp552-Luc or CYP1A1-Luc and AhR and Arnt, and the cells were then exposed to TCDD stimulation. Clear TCDD-induced CYP1A1 promoter activity was observed in HSY cells (Fig. 5A), and Zp552-Luc activity was also enhanced by TCDD (Fig. 5B).

To confirm the role of the AhR/Arnt complex, we transfected different quantities of AhR and Arnt into HSY cells. The TCDD (10 nM) treatment-induced Zp activity was dependent on the levels of transfected AhR and Arnt (Fig. 5C). The range of TCDD required

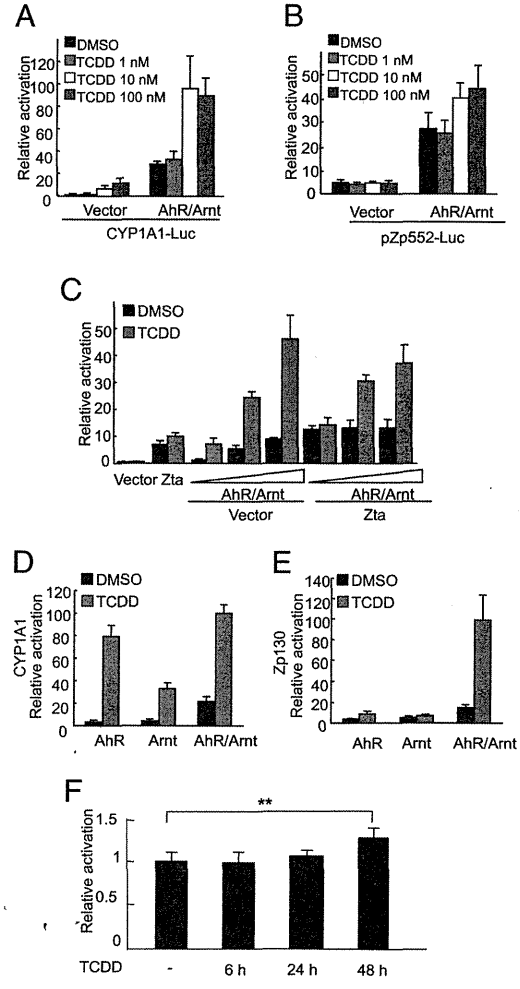

FIGURE 5. Transcriptional activation of the CYP1A1 promoter or Zp in response to TCDD in salivary epithelial cells and HepG2 cells. (**A–E**) HSY cells transiently cotransfected with CYP1A1-Luc (A, D), pZp552-Luc (B, C), or pZp130-Luc (E) and plasmids encoding human AhR and/or Arnt. (C) Increasing amounts of plasmids encoding human AhR and Arnt (0.05–0.25 μg) were cotransfected with or without Zta. (**F**) HepG2 cells were transfected with Zp130-Luc. Luciferase activities were measured after 48 h stimulation with increasing amounts of TCDD (1–100 nM) (A, B) or 10 nM TCDD (C–F). Data were averaged over at least three experiments. Values represent means ± SD derived from normalized data, with transfections performed in triplicate in each experiment. $**p < 0.01$.

for both the activation of the CYP1A1 promoter and for the activation of Zp was similar. Although CYP1A1 promoter activity was increased by either AhR or Arnt (Fig. 5D), an increase in Zp130 activity was observed only upon the exogenous expression of both AhR and Arnt (Fig. 5E). Zp contains the autoreactive sequence sites ZIIIA and ZIIIB; therefore, the exogenous expression of the BZLF1 gene product Zta increased the activity of Zp (Fig. 5C). The Zp activity induced by TCDD-activated AhR/Arnt was not enhanced by Zta expression (Fig. 5C). These results demonstrate that Zp activity is stimulated by TCDD via the AhR/Arnt complex and that this stimulation represents a distinct transcriptional mechanism that occurs via CYP1A1 promoter activation. Moreover, the endogenous expression of AhR/Arnt in HepG2 cells is also responsive for Zp transactivation by TCDD (Fig. 5F). This activity was not dramatic but was still significant.

Identification of the cis*-acting AhR-responsive region in Zp*

To investigate the activation of the AhR-responsive regions in Zp, we generated a series of deletion plasmids encompassing the −551- to +13-bp region of Zp flanked by the luciferase-coding region (Fig. 1).

We cotransfected HSY cells with pZp130-Luc, pZp221-Luc, or pZp552-Luc and AhR and Arnt. The TCDD-induced Zp552-Luc and Zp221-Luc activities were similar, whereas the shortest plasmid, pZp130-Luc, showed the highest level of activation in response to TCDD (Fig. 6A). A TCDD concentration of >10 nM was required to activate pZp130-Luc (Fig. 6B); the same concentration was required to activate pZp552-Luc and CYP1A1-Luc (Fig. 5A, 5B). To confirm the presence of AhR *cis*-response elements in Zp130, we generated the deletion mutant plasmid pZp552Δ130-Luc by eliminating the −130- to −44-bp region from the intact pZp552-Luc plasmid. TCDD failed to activate pZp552Δ130-Luc in HSY cells (Fig. 6C). Exogenously expressed Zta also failed to stimulate this promoter because the Zta binding sites ZIIIA and ZIIIB are located between −134 and −104 bp (Fig. 6C). The serially mutated reporter plasmids MI, MII, and MIII (Fig. 1) exhibited an incomplete loss of promoter activity in comparison with intact pZp552-Luc (Fig. 6D). These results indicate that the putative location of the AhR response element is proximal to the transcription start site within a 130-bp segment of the Zp.

Coexpression of AhR and Arnt is required for Zp activation (Fig. 5E). The AhR/Arnt heterodimer binds specific xenobiotic response elements containing core motifs (5′-GCGTG-3′) in responsive genes, modulating their expression. Although there is no core sequence for AhR in the Zp region, we attempted to evaluate the binding of TCDD-activated AhR/Arnt to the Zp130 fragment using an EMSA. Nuclear extracts from TCDD-treated HSY cells that ectopically expressed AhR and Arnt showed that AhR/Arnt bound to Zp130. This binding was specifically inhibited by nonlabeled Zp130 (Fig. 6E). This result suggests a physical interaction between the AhR/Arnt complex and Zp130. A luciferase assay conducted using a deletion mutant of pZp552-Luc demonstrated that ligand-activated AhR interacts primarily with the ZII element (Fig. 6D), which also binds to basic leucine zipper transcription factors such as ATF1, CREB, and ATF2 (35). Future studies will be necessary to define the AhR binding sites within Zp.

AhR activation is associated with EBV reactivation in SS

SS is a systemic autoimmune disorder that affects the salivary and lacrimal glands and causes mononuclear cell infiltration, causing

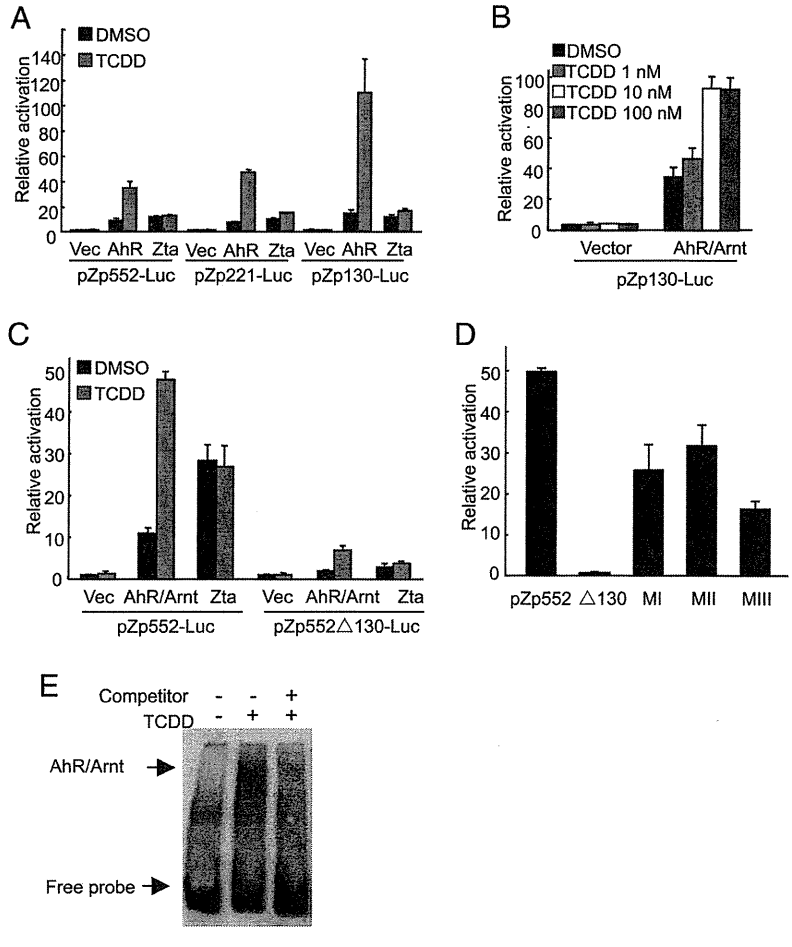

FIGURE 6. The region of Zp required for response to TCDD-activated AhR in HSY cells. (**A–D**) Luciferase activities were measured after 48 h stimulation with TCDD with or without exogenous human AhR and Arnt or Zta in HSY cells. The plasmid pZp552Δ130-Luc, which lacked bases −130 to −40 from the original pZp553-Luc (C, D), and deletion mutants MI, MII, or MIII (D) are shown in Fig. 1. Values represent means ± SD derived from normalized data, with transfections performed in triplicate in each experiment. Data were averaged over at least three experiments. (**E**) Ad-AhR– and Ad-Arnt–infected HSY cells were incubated for 2 h in the presence of vehicle (0.001%) or TCDD (10 nM). The nuclear extract was incubated for 20 min with 20 fmol biotin-labeled Zp130 probe and then subjected to EMSA. The specificity of AhR DNA binding was determined by competition reactions with 4 pmol of unlabeled Zp130.

the clinical symptoms of dryness of the mouth and eyes. The pathogenesis of SS remains unclear; however, a high incidence of EBV reactivation in SS has been reported. EBV Ags and DNA are present in the infiltrating lymphocytes and salivary gland epithelial cells of SS patients (22, 24). Infectious EBV is present in the saliva of SS patients (21, 36) and in the culture supernatants of B cell lines established from SS patients (23). Thus, EBV reactivation in SS is thought to contribute to the initiation or perpetuation of tissue destruction in target organs such as the salivary and lacrimal glands. To detect AhR ligands in the saliva of SS patients, we conducted a reporter assay for the CYP1A1 promoter and Zp. As disease controls, we assessed DM patients with levels of saliva secretion similar to those of SS patients. In this study, we found that Zp130 was strongly activated by the saliva of SS patients in the presence of exogenous AhR expression, whereas activation in the saliva of NML or DM individuals was basal level (Fig. 7A). The saliva from SS patients also activated the CYP1A1 promoter in the presence of exogenous AhR expression (Fig. 7B), and this activity was significantly weaker in the saliva of NML and DM individuals. Moreover, there was a positive correlation between the Zp and CYP1A1 promoter activities (Fig. 7C). These results indicate that the AhR ligand in the saliva of SS patients may stimulate BZLF1 transactivation.

The relationship between AhR activation and autoantibodies in SS

The most common autoantibodies in patients with SS are those directed against the SSA/Ro and SSB/La ribonucleoprotein complexes (37, 38). These Abs are detected in serum and can be produced locally in the affected salivary glands (39). Anti-SSB/La Abs are accompanied by anti-SSA/Ro Abs, whereas anti-SSA/Ro Abs can be found either with or without anti-SSB/La Abs (40). In this study, serum titers of anti-SSA/Ro and anti-SSB/La Abs were evaluated relative to Zp and CYP1A1 promoter activities. Although a high titer of anti-SSB/La Ab was detected in only 6 of 19 patients (Table I), the Ab titer was correlated with Zp and CYP1A1 promoter activities in these patients (Fig. 8A, 8B).

Discussion

Several epidemiological studies suggest an association between dioxin exposure and an increased incidence of certain human diseases. After an industrial accident in Seveso, Italy, in which workers were acutely exposed to high levels of TCDD, a high incidence of gastrointestinal, lymphatic, and hematopoietic cancers and endocrine and immunological effects was observed (41). The long-term effects of dioxin exposure include an excess of lymphohematopoietic neoplasms, such as Hodgkin's and non-Hodgkin's lymphoma (42). EBV has been associated with certain types of non-Hodgkin's lymphoma, such as Burkitt's lymphoma and lymphomas related to severe immunosuppression (43). Dioxins in adipose tissue and Abs against Epstein–Barr early Ag were investigated in non-Hodgkin's lymphoma patients. An increased risk of non-Hodgkin's lymphoma was found for patients in the high-concentration and high-titer group (44). The level of early Ag Abs reflects the degree of EBV viral replication, a relationship that was also observed in SS patients. Moreover, a high early Ag Ab titer was frequently detected in SS patients who developed non-Hodgkin's lymphoma (45, 46). The present study demonstrates that environmental contaminants such as dioxins may induce EBV reactivation and thus act as risk factors for SS.

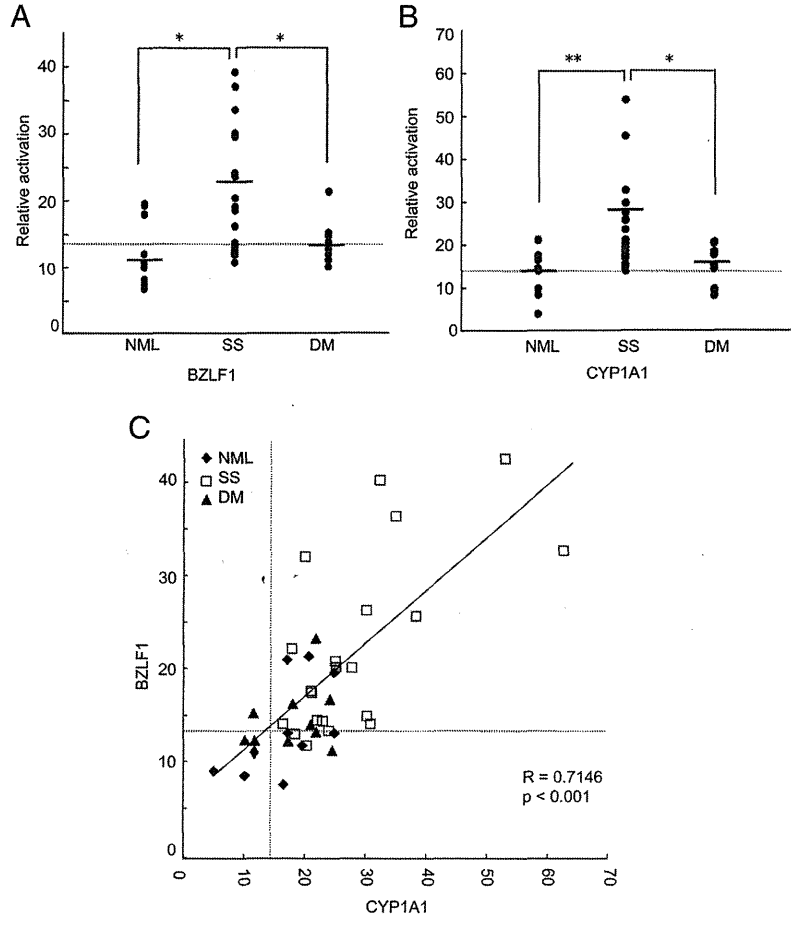

FIGURE 7. Zp and CYP1A1 promoter activation by SS saliva. pZp130-Luc (**A**) or CYP1A1-Luc (**B**) was cotransfected with plasmids encoding human AhR and Arnt into HSY cells, followed by stimulation with NML, SS, and non-SS DM saliva. Luciferase activities were measured after 48 h stimulation. (**C**) A statistically significant correlation between Zp130 (A) and CYP1A1 activities (B). The activities of each promoter were expressed as the relative activity with respect to the activity induced by 100 nM TCDD, which was set to a value of 100. The baseline of this assay, derived from DMSO alone, is indicated by the dotted lines. Statistical analysis was performed using one-way ANOVA and the Pearson correlation test. $*p < 0.05$, $**p < 0.005$.

Table I. Clinical information on patients and summary of data obtained by luciferase assay

Patient No.	Age (y)	Sex	Autoantibody		Luciferase Assay	
			SSA/Ro	SSB/La	BZLF1	CYP1A1
SS 01	55	F	23.8	6.4	23.4	39.2
SS 02	34	F	ND	ND	38.8	54.3
SS 03	76	F	500.0	7.0	13.6	30.9
SS 04	72	F	500.0	7.0	10.7	20.6
SS 05	70	F	ND	ND	19.0	25.6
SS 06	70	F	500.0	7.0	36.7	33.0
SS 07	72	F	7.0	7.0	20.2	18.2
SS 08	72	F	ND	ND	18.3	28.3
SS 09	69	F	107.7	7.0	13.0	16.8
SS 10	68	F	500.0	474.6	24.0	30.8
SS 11	58	F	500.0	132.2	29.3	20.4
SS 12	52	F	500.0	341.0	29.8	64.2
SS 13	52	F	500.0	ND	12.1	24.5
SS 14	58	F	500.0	500.0	33.3	35.8
SS 15	71	F	476.0	32.0	13.1	23.4
SS 16	66	F	500.0	27.1	16.1	21.4
SS 17	37	F	500.0	7.0	11.8	18.8
SS 18	58	F	307.0	ND	13.2	22.5
SS 19	70	F	ND	ND	12.5	31.1

In this study, we studied ligand-activated AhR using a Zp reporter assay that involved the modification of chemically activated luciferase gene expression (CALUX). The CALUX method is becoming increasingly common for the evaluation of dioxins in blood (47), milk (48), food (49), and environmental samples (50). The conventional method, high-resolution chromatography/mass spectrometry, is time-consuming, costly, and requires large sample volumes. A previous comparison of results obtained using the two assays revealed few differences (51). For our assessments, involving limited volumes of saliva, the CALUX bioassay was a useful tool for evaluating dioxins.

In B cells, the observed mechanisms of EBV reactivation in vitro are hypothesized to involve the activation of BZLF1 transcription by TPA, *N*-butyric acid, or Ig–cross-linking Abs. However, the priming factor for EBV reactivation in vivo is poorly understood. The plasma cell differentiation factor X-box binding protein-1 (XBP-1) binds and transactivates Zp in a plasma cell line and in lymphoid cell lines but not in epithelial cell lines (52). XBP-1 also induces BZLF1 transcription and is involved in B cell differentiation into plasma cells. In this study, we propose a new candidate dioxin that induces BZLF1 in both activated B cells and salivary epithelial cells. In contrast to XBP-1, the response to TCDD-activated AhR was higher in salivary epithelial cells than in activated B cells. Activated B cells have increased AhR mRNA levels and protein expression (27) and are more responsive to TCDD than are nonactivated B cells (29). Chen and Tukey (53) reported that TPA, as a protein kinase C activator, enhances CYP1A1 gene transcription by AhR, indicating that protein kinase C promotes nuclear events that work in concert with or precede AhR binding to the gene. This result suggests that the B cells that are responsible for TCDD after TPA stimulation may use the protein kinase C signaling pathway.

EBNA-3 is an EBV-encoded nuclear Ag that is indispensable for B cell transformation and is implicated in the maintenance of lymphoblastoid cell line proliferation. The overexpression of EBNA-3 induces G_0/G_1 arrest (54), and the elimination of EBNA-3 results in cell death (55) in lymphoblastoid cell lines. EBNA-3 directly interacts with AhR and enhances its transactivational function via the ligand-activated AhR (56). TCDD-activated AhR induces cell cycle arrest at G_1, accompanied by the increased expression of the CDK2 inhibitor $p27^{kip1}$ (57). Studies of murine B cell development have shown that AhR ligands, such as polycyclic aromatic compounds, induce apoptosis in pro- and pre-B cells (58). The function of AhR in cell cycle progression is also consistent with its interaction with proteins such as pRb (59) and the p65 subunit of NF-κB RelA (60). Although the molecular mechanisms underlying its activity are not understood, EBNA-3 compromises the inhibitory effect of TCDD on the growth of EBV-positive lymphoblasts (56). All of the latent EBV genes, including

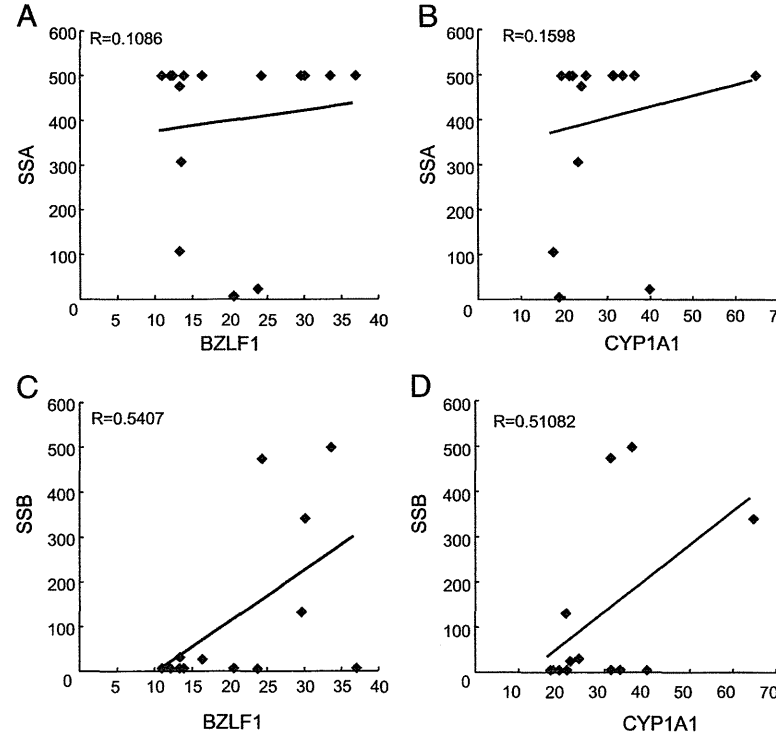

FIGURE 8. Analysis of the correlation between autoantibody titer and AhR transactivation in SS patients. The titer of anti-SSA/Ro (**A**, **B**) or SSB/La (**C**, **D**) autoantibodies in SS sera was compared with the corresponding Zp (A, C) (Fig. 7A) or CYP1A1 (B, D) (Fig. 7B) promoter activities. Statistical analysis was performed using a Pearson correlation test.

EBNA-3, are expressed in EBV$^+$ naive (IgD$^+$) B cells (latency III). Latency III is known as the growth program because EBV-transformed B cells proliferating in vitro exhibit this expression pattern (61). In germinal center B cells, EBV gene expression is restricted to EBNA1, LMP1, and LMP2 (latency II) (62). In the peripheral blood, EBV exists within the IgD$^-$ memory B cell pool, with expression more restricted to LMP2A (latency 0) (8). However, EBV status in the salivary glands has not been elucidated. In this study, we used EBV-positive B cell lines B95-8 and P3HR1, which express latency III and latency II patterns, respectively. This finding suggests that EBNA-3 may cause different Zp sensitivity toward TCDD-activated AhR in B95-8 and P3HR1 (Figs. 3, 4).

Our previous study demonstrated that Zp221 activity and BZLF1 transcription were induced by saliva from SS patients (63). TGF-β1, which is expressed in SS salivary glands, induced Zp221 activity via the MAPK signaling pathway. These data suggest that EBV reactivation at the inflammatory site may occur because of the presence of TGF-β1. In the present study, we observed TCDD-induced AhR-dependent Zp activity. Thus, TCDD may be a trigger for EBV reactivation without inflammation.

AhR has been shown to regulate the level of T regulatory and Th17 cell differentiation and to modulate the severity of experimental autoimmune encephalitis in a ligand-dependent manner in mice (64–66). Human CD4 cells derived from healthy donors produced IL-22 but not IL-17 in response to ligand-activated AhR (67, 68). Human exposure to an extremely high dose of TCDD in vivo induced a selective increase in the frequency of T cells producing IL-22 but not IL-17, IL-10, or IFN-γ (69). Activated AhR also promoted T cell differentiation into functional Foxp3$^+$ human induced regulatory T cells, which produce IL-10 in vitro (70). More recently, Li et al. (71) showed that intraepithelial lymphocytes express high levels of AhR and that receptor activation directly affects the maintenance but not the development, homing, or proliferation of intraepithelial lymphocytes. AhR activity can be regulated by certain dietary components derived from vegetables, which may regulate the intestinal immune system. Currently, it is not clear why AhR activation can either increase or reduce inflammatory reactions. We hypothesize that the immunological condition of the host may contribute to the pathogenesis of autoimmune diseases involving EBV reactivation caused by activated AhR.

SS is a chronic autoimmune disease that is characterized by the presence of a variety of autoantibodies directed against organ-specific and non–organ-specific autoantigens. The most common of these Abs are directed against two ribonucleoprotein Ags known as SSA/Ro and SSB/La. It is still unknown whether any of the autoantibodies have a pathogenic potential or whether they are all part of a secondary response to salivary glands already damaged by other processes. Anti-SSA/Ro and anti-SSB/La are found in the saliva of SS patients (72), and the B cells that infiltrate the salivary glands contain intracytoplasmic Igs with anti-SSA/Ro and anti-SSB/La activity (39, 73, 74). In this case, ectopic lymphoid germinal centers that contain Ag-presenting dendritic cells, T cells, and B cells have been found, providing a microenvironment that is conducive to the propagation of the autoimmune response (39). Finally, an increased production of SSB/La mRNA in acinar epithelial cells has been observed (75), and translocation and membrane localization of the SSB/La protein has been observed in conjunctival epithelial cells of SS patients (76). These reports suggest that anti-SSA/Ro and anti-SSB/La Abs may participate in the local immune response in the affected exocrine glands. In the present study, we found a correlation between anti-SSB/La in the sera and AhR activation by saliva in SS patients. These data lead us to speculate that EBV reactivation induced by dioxins may cause an immune response in the salivary glands of SS patients.

Acknowledgments

We thank N. Tanese and M.J. Garabedian (New York University, New York, NY) for helpful advice and comments.

Disclosures

The authors have no financial conflicts of interest.

References

1. Schmidt, J. V., and C. A. Bradfield. 1996. Ah receptor signaling pathways. *Annu. Rev. Cell Dev. Biol.* 12: 55–89.
2. Rowlands, J. C., and J. A. Gustafsson. 1997. Aryl hydrocarbon receptor-mediated signal transduction. *Crit. Rev. Toxicol.* 27: 109–134.
3. Couture, L. A., B. D. Abbott, and L. S. Birnbaum. 1990. A critical review of the developmental toxicity and teratogenicity of 2,3,7,8-tetrachlorodibenzo-*p*-dioxin: recent advances toward understanding the mechanism. *Teratology* 42: 619–627.
4. Burleson, G. R., H. Lebrec, Y. G. Yang, J. D. Ibanes, K. N. Pennington, and L. S. Birnbaum. 1996. Effect of 2,3,7,8-tetrachlorodibenzo-p-dioxin (TCDD) on influenza virus host resistance in mice. *Fundam. Appl. Toxicol.* 29: 40–47.
5. Murayama, T., M. Inoue, T. Nomura, S. Mori, and Y. Eizuru. 2002. 2,3,7,8-Tetrachlorodibenzo-*p*-dioxin is a possible activator of human cytomegalovirus replication in a human fibroblast cell line. *Biochem. Biophys. Res. Commun.* 296: 651–656.
6. Ohata, H., T. Tetsuka, H. Hayashi, K. Onozaki, and T. Okamoto. 2003. 3-Methylcholanthrene activates human immunodeficiency virus type 1 replication via aryl hydrocarbon receptor. *Microbiol. Immunol.* 47: 363–370.
7. Garssen, J., H. Van der Vliet, A. De Klerk, W. Goettsch, J. A. Dormans, C. A. Bruggeman, A. D. Osterhaus, and H. Van Loveren. 1995. A rat cytomegalovirus infection model as a tool for immunotoxicity testing. *Eur. J. Pharmacol.* 292: 223–231.
8. Babcock, G. J., L. L. Decker, M. Volk, and D. A. Thorley-Lawson. 1998. EBV persistence in memory B cells in vivo. *Immunity* 9: 395–404.
9. Münz, C., J. D. Lünemann, M. T. Getts, and S. D. Miller. 2009. Antiviral immune responses: triggers of or triggered by autoimmunity? *Nat. Rev. Immunol.* 9: 246–258.
10. Countryman, J., and G. Miller. 1985. Activation of expression of latent Epstein-Barr herpesvirus after gene transfer with a small cloned subfragment of heterogeneous viral DNA. *Proc. Natl. Acad. Sci. USA* 82: 4085–4089.
11. Rooney, C. M., D. T. Rowe, T. Ragot, and P. J. Farrell. 1989. The spliced BZLF1 gene of Epstein-Barr virus (EBV) transactivates an early EBV promoter and induces the virus productive cycle. *J. Virol.* 63: 3109–3116.
12. Speck, S. H., T. Chatila, and E. Flemington. 1997. Reactivation of Epstein-Barr virus: regulation and function of the BZLF1 gene. *Trends Microbiol.* 5: 399–405.
13. Flemington, E., and S. H. Speck. 1990. Identification of phorbol ester response elements in the promoter of Epstein-Barr virus putative lytic switch gene BZLF1. *J. Virol.* 64: 1217–1226.
14. Montalvo, E. A., M. Cottam, S. Hill, and Y. J. Wang. 1995. YY1 binds to and regulates *cis*-acting negative elements in the Epstein-Barr virus BZLF1 promoter. *J. Virol.* 69: 4158–4165.
15. zur Hausen, H., F. J. O'Neill, U. K. Freese, and E. Hecker. 1978. Persisting oncogenic herpesvirus induced by the tumour promotor TPA. *Nature* 272: 373–375.
16. Takada, K. 1984. Cross-linking of cell surface immunoglobulins induces Epstein-Barr virus in Burkitt lymphoma lines. *Int. J. Cancer* 33: 27–32.
17. Luka, J., B. Kallin, and G. Klein. 1979. Induction of the Epstein-Barr virus (EBV) cycle in latently infected cells by n-butyrate. *Virology* 94: 228–231.
18. Sulentic, C. E., M. P. Holsapple, and N. E. Kaminski. 1998. Aryl hydrocarbon receptor-dependent suppression by 2,3,7, 8-tetrachlorodibenzo-*p*-dioxin of IgM secretion in activated B cells. *Mol. Pharmacol.* 53: 623–629.
19. Crawford, D. H., and I. Ando. 1986. EB virus induction is associated with B-cell maturation. *Immunology* 59: 405–409.
20. Fox, R. I., T. Bumol, R. Fantozzi, R. Bone, and R. Schreiber. 1986. Expression of histocompatibility antigen HLA-DR by salivary gland epithelial cells in Sjögren's syndrome. *Arthritis Rheum.* 29: 1105–1111.
21. Fox, R. I., G. Pearson, and J. H. Vaughan. 1986. Detection of Epstein-Barr virus-associated antigens and DNA in salivary gland biopsies from patients with Sjogren's syndrome. *J. Immunol.* 137: 3162–3168.
22. Saito, I., B. Servenius, T. Compton, and R. I. Fox. 1989. Detection of Epstein-Barr virus DNA by polymerase chain reaction in blood and tissue biopsies from patients with Sjogren's syndrome. *J. Exp. Med.* 169: 2191–2198.
23. Tateishi, M., I. Saito, K. Yamamoto, and N. Miyasaka. 1993. Spontaneous production of Epstein-Barr virus by B lymphoblastoid cell lines obtained from patients with Sjögren's syndrome: possible involvement of a novel strain of Epstein-Barr virus in disease pathogenesis. *Arthritis Rheum.* 36: 827–835.
24. Mariette, X., J. Gozlan, D. Clerc, M. Bisson, and F. Morinet. 1991. Detection of Epstein-Barr virus DNA by in situ hybridization and polymerase chain reaction in salivary gland biopsy specimens from patients with Sjögren's syndrome. *Am. J. Med.* 90: 286–294.
25. Yanagawa, T., Y. Hayashi, S. Nagamine, H. Yoshida, Y. Yura, and M. Sato. 1986. Generation of cells with phenotypes of both intercalated duct-type and myoepithelial cells in human parotid gland adenocarcinoma clonal cells grown in athymic nude mice. *Virchows Arch. B Cell Pathol. Incl. Mol. Pathol.* 51: 187–195.

26. Karras, J. G., and M. P. Holsapple. 1994. Mechanisms of 2,3,7,8-tetrachlorodibenzo-*p*-dioxin (TCDD)-induced disruption of B-lymphocyte signaling in the mouse: a current perspective. *Exp. Clin. Immunogenet.* 11: 110–118.
27. Allan, L. L., and D. H. Sherr. 2005. Constitutive activation and environmental chemical induction of the aryl hydrocarbon receptor/transcription factor in activated human B lymphocytes. *Mol. Pharmacol.* 67: 1740–1750.
28. Crawford, R. B., M. P. Holsapple, and N. E. Kaminski. 1997. Leukocyte activation induces aryl hydrocarbon receptor up-regulation, DNA binding, and increased Cyp1a1 expression in the absence of exogenous ligand. *Mol. Pharmacol.* 52: 921–927.
29. Morris, D. L., J. G. Karras, and M. P. Holsapple. 1993. Direct effects of 2,3,7,8-tetrachlorodibenzo-*p*-dioxin (TCDD) on responses to lipopolysaccharide (LPS) by isolated murine B-cells. *Immunopharmacology* 26: 105–112.
30. Laichalk, L. L., and D. A. Thorley-Lawson. 2005. Terminal differentiation into plasma cells initiates the replicative cycle of Epstein-Barr virus in vivo. *J. Virol.* 79: 1296–1307.
31. Hadinoto, V., M. Shapiro, C. C. Sun, and D. A. Thorley-Lawson. 2009. The dynamics of EBV shedding implicate a central role for epithelial cells in amplifying viral output. *PLoS Pathog.* 5: e1000496.
32. Sixbey, J. W., J. G. Nedrud, N. Raab-Traub, R. A. Hanes, and J. S. Pagano. 1984. Epstein-Barr virus replication in oropharyngeal epithelial cells. *N. Engl. J. Med.* 310: 1225–1230.
33. Wolf, H., M. Haus, and E. Wilmes. 1984. Persistence of Epstein-Barr virus in the parotid gland. *J. Virol.* 51: 795–798.
34. Hoover, S. E., J. Kawada, W. Wilson, and J. I. Cohen. 2008. Oropharyngeal shedding of Epstein-Barr virus in the absence of circulating B cells. *J. Infect. Dis.* 198: 318–323.
35. Ruf, I. K., and D. R. Rawlins. 1995. Identification and characterization of ZIIBC, a complex formed by cellular factors and the ZII site of the Epstein-Barr virus BZLF1 promoter. *J. Virol.* 69: 7648–7657.
36. Saito, I., S. Nishimura, I. Kudo, R. I. Fox, and I. Moro. 1991. Detection of Epstein-Barr virus and human herpes virus type 6 in saliva from patients with lymphoproliferative diseases by the polymerase chain reaction. *Arch. Oral Biol.* 36: 779–784.
37. Fox, R. I., M. Stern, and P. Michelson. 2000. Update in Sjögren syndrome. *Curr. Opin. Rheumatol.* 12: 391–398.
38. Fox, R. I. 2005. Sjögren's syndrome. *Lancet* 366: 321–331.
39. Salomonsson, S., M. V. Jonsson, K. Skarstein, K. A. Brokstad, P. Hjelmström, M. Wahren-Herlenius, and R. Jonsson. 2003. Cellular basis of ectopic germinal center formation and autoantibody production in the target organ of patients with Sjögren's syndrome. *Arthritis Rheum.* 48: 3187–3201.
40. Routsias, J. G., and A. G. Tzioufas. 2007. Sjögren's syndrome: study of autoantigens and autoantibodies. *Clin. Rev. Allergy Immunol.* 32: 238–251.
41. Bertazzi, P. A., I. Bernucci, G. Brambilla, D. Consonni, and A. C. Pesatori. 1998. The Seveso studies on early and long-term effects of dioxin exposure: a review. *Environ. Health Perspect.* 106(Suppl 2): 625–633.
42. Bertazzi, P. A., D. Consonni, S. Bachetti, M. Rubagotti, A. Baccarelli, C. Zocchetti, and A. C. Pesatori. 2001. Health effects of dioxin exposure: a 20-year mortality study. *Am. J. Epidemiol.* 153: 1031–1044.
43. Okano, M., G. M. Thiele, J. R. Davis, H. L. Grierson, and D. T. Purtilo. 1988. Epstein-Barr virus and human diseases: recent advances in diagnosis. *Clin. Microbiol. Rev.* 1: 300–312.
44. Hardell, L., G. Lindström, B. van Bavel, K. Hardell, A. Linde, M. Carlberg, and G. Liljegren. 2001. Adipose tissue concentrations of dioxins and dibenzofurans, titers of antibodies to Epstein-Barr virus early antigen and the risk for non-Hodgkin lymphoma. *Environ. Res.* 87: 99–107.
45. Fox, R. I., I. Saito, E. K. Chan, S. Josephs, S. Z. Salahuddin, D. V. Ahlashi, F. W. Staal, R. Gallo, H. Pei-Ping, and C. S. Le. 1989. Viral genomes in lymphomas of patients with Sjögren's syndrome. *J. Autoimmun.* 2: 449–455.
46. Fox, R. I., M. Luppi, H. I. Kang, and P. Pisa. 1991. Reactivation of Epstein-Barr virus in Sjögren's syndrome. *Springer Semin. Immunopathol.* 13: 217–231.
47. Van Wouwe, N., I. Windal, H. Vanderperren, G. Eppe, C. Xhrouet, A. C. Massart, N. Debacker, A. Sasse, W. Baeyens, E. De Pauw, et al. 2004. Validation of the CALUX bioassay for PCDD/F analyses in human blood plasma and comparison with GC-HRMS. *Talanta* 63: 1157–1167.
48. Laier, P., T. Cederberg, J. C. Larsen, and A. M. Vinggaard. 2003. Applicability of the CALUX bioassay for screening of dioxin levels in human milk samples. *Food Addit. Contam.* 20: 583–595.
49. Tsutsumi, T., Y. Amakura, M. Nakamura, D. J. Brown, G. C. Clark, K. Sasaki, M. Toyoda, and T. Maitani. 2003. Validation of the CALUX bioassay for the screening of PCDD/Fs and dioxin-like PCBs in retail fish. *Analyst (Lond.)* 128: 486–492.
50. Joung, K. E., Y. H. Chung, and Y. Y. Sheen. 2007. DRE-CALUX bioassay in comparison with HRGC/MS for measurement of toxic equivalence in environmental samples. *Sci. Total Environ.* 372: 657–667.
51. Nording, M., M. S. Denison, D. Baston, Y. Persson, E. Spinnel, and P. Haglund. 2007. Analysis of dioxins in contaminated soils with the calux and caflux bioassays, an immunoassay, and gas chromatography/high-resolution mass spectrometry. *Environ. Toxicol. Chem.* 26: 1122–1129.
52. Sun, C. C., and D. A. Thorley-Lawson. 2007. Plasma cell-specific transcription factor XBP-1s binds to and transactivates the Epstein-Barr virus BZLF1 promoter. *J. Virol.* 81: 13566–13577.
53. Chen, Y. H., and R. H. Tukey. 1996. Protein kinase C modulates regulation of the CYP1A1 gene by the aryl hydrocarbon receptor. *J. Biol. Chem.* 271: 26261–26266.
54. Cooper, A., E. Johannsen, S. Maruo, E. Cahir-McFarland, D. Illanes, D. Davidson, and E. Kieff. 2003. EBNA3A association with RBP-Jκ downregulates c-myc and Epstein-Barr virus-transformed lymphoblast growth. *J. Virol.* 77: 999–1010.
55. Maruo, S., E. Johannsen, D. Illanes, A. Cooper, and E. Kieff. 2003. Epstein-Barr virus nuclear protein EBNA3A is critical for maintaining lymphoblastoid cell line growth. *J. Virol.* 77: 10437–10447.
56. Kashuba, E. V., K. Gradin, M. Isaguliants, L. Szekely, L. Poellinger, G. Klein, and A. Kazlauskas. 2006. Regulation of transactivation function of the aryl hydrocarbon receptor by the Epstein-Barr virus-encoded EBNA-3 protein. *J. Biol. Chem.* 281: 1215–1223.
57. Kolluri, S. K., C. Weiss, A. Koff, and M. Göttlicher. 1999. p27(Kip1) induction and inhibition of proliferation by the intracellular Ah receptor in developing thymus and hepatoma cells. *Genes Dev.* 13: 1742–1753.
58. Yamaguchi, K., R. I. Near, R. A. Matulka, A. Shneider, P. Toselli, A. F. Trombino, and D. H. Sherr. 1997. Activation of the aryl hydrocarbon receptor/transcription factor and bone marrow stromal cell-dependent preB cell apoptosis. *J. Immunol.* 158: 2165–2173.
59. Ge, N. L., and C. J. Elferink. 1998. A direct interaction between the aryl hydrocarbon receptor and retinoblastoma protein: linking dioxin signaling to the cell cycle. *J. Biol. Chem.* 273: 22708–22713.
60. Tian, Y., S. Ke, M. S. Denison, A. B. Rabson, and M. A. Gallo. 1999. Ah receptor and NF-κB interactions, a potential mechanism for dioxin toxicity. *J. Biol. Chem.* 274: 510–515.
61. Joseph, A. M., G. J. Babcock, and D. A. Thorley-Lawson. 2000. Cells expressing the Epstein-Barr virus growth program are present in and restricted to the naive B-cell subset of healthy tonsils. *J. Virol.* 74: 9964–9971.
62. Babcock, G. J., D. Hochberg, and A. D. Thorley-Lawson. 2000. The expression pattern of Epstein-Barr virus latent genes in vivo is dependent upon the differentiation stage of the infected B cell. *Immunity* 13: 497–506.
63. Nagata, Y., H. Inoue, K. Yamada, H. Higashiyama, K. Mishima, Y. Kizu, I. Takeda, F. Mizuno, Y. Hayashi, and I. Saito. 2004. Activation of Epstein-Barr virus by saliva from Sjogren's syndrome patients. *Immunology* 111: 223–229.
64. Funatake, C. J., N. B. Marshall, L. B. Steppan, D. V. Mourich, and N. I. Kerkvliet. 2005. Cutting edge: activation of the aryl hydrocarbon receptor by 2,3,7,8-tetrachlorodibenzo-*p*-dioxin generates a population of $CD4^+$ $CD25^+$ cells with characteristics of regulatory T cells. *J. Immunol.* 175: 4184–4188.
65. Quintana, F. J., A. S. Basso, A. H. Iglesias, T. Korn, M. F. Farez, E. Bettelli, M. Caccamo, M. Oukka, and H. L. Weiner. 2008. Control of T_{reg} and T_H17 cell differentiation by the aryl hydrocarbon receptor. *Nature* 453: 65–71.
66. Veldhoen, M., K. Hirota, A. M. Westendorf, J. Buer, L. Dumoutier, J. C. Renauld, and B. Stockinger. 2008. The aryl hydrocarbon receptor links TH17-cell-mediated autoimmunity to environmental toxins. *Nature* 453: 106–109.
67. Trifari, S., C. D. Kaplan, E. H. Tran, N. K. Crellin, and H. Spits. 2009. Identification of a human helper T cell population that has abundant production of interleukin 22 and is distinct from T_H-17, T_H1 and T_H2 cells. *Nat. Immunol.* 10: 864–871.
68. Ramirez, J. M., N. C. Brembilla, O. Sorg, R. Chicheportiche, T. Matthes, J. M. Dayer, J. H. Saurat, E. Roosnek, and C. Chizzolini. 2010. Activation of the aryl hydrocarbon receptor reveals distinct requirements for IL-22 and IL-17 production by human T helper cells. *Eur. J. Immunol.* 40: 2450–2459.
69. Brembilla, N. C., J. M. Ramirez, R. Chicheportiche, O. Sorg, J. H. Saurat, and C. Chizzolini. 2011. In vivo dioxin favors interleukin-22 production by human $CD4^+$ T cells in an aryl hydrocarbon receptor (AhR)-dependent manner. *PLoS ONE* 6: e18741.
70. Gandhi, R., D. Kumar, E. J. Burns, M. Nadeau, B. Dake, A. Laroni, D. Kozoriz, H. L. Weiner, and F. J. Quintana. 2010. Activation of the aryl hydrocarbon receptor induces human type 1 regulatory T cell-like and $Foxp3^+$ regulatory T cells. *Nat. Immunol.* 11: 846–853.
71. Li, Y., S. Innocentin, D. R. Withers, N. A. Roberts, A. R. Gallagher, E. F. Grigorieva, C. Wilhelm, and M. Veldhoen. 2011. Exogenous stimuli maintain intraepithelial lymphocytes via aryl hydrocarbon receptor activation. *Cell* 147: 629–640.
72. Hammi, A. R., I. H. Al-Hashimi, M. E. Nunn, and M. Zipp. 2005. Assessment of SS-A and SS-B in parotid saliva of patients with Sjögren's syndrome. *J. Oral Pathol. Med.* 34: 198–203.
73. Schwarzmann, F., N. Prang, B. Reichelt, B. Rinkes, S. Haist, M. Marschall, and H. Wolf. 1994. Negatively *cis*-acting elements in the distal part of the promoter of Epstein-Barr virus *trans*-activator gene BZLF1. *J. Gen. Virol.* 75: 1999–2006.
74. Halse, A., J. B. Harley, U. Kroneld, and R. Jonsson. 1999. Ro/SS-A-reactive B lymphocytes in salivary glands and peripheral blood of patients with Sjögren's syndrome. *Clin. Exp. Immunol.* 115: 203–207.
75. Tzioufas, A. G., I. Hantoumi, M. Polihronis, G. Xanthou, and H. M. Moutsopoulos. 1999. Autoantibodies to La/SSB in patients with primary Sjögren's syndrome (pSS) are associated with upregulation of La/SSB mRNA in minor salivary gland biopsies (MSGs). *J. Autoimmun.* 13: 429–434.
76. Yannopoulos, D. I., S. Roncin, A. Lamour, Y. L. Pennec, H. M. Moutsopoulos, and P. Youinou. 1992. Conjunctival epithelial cells from patients with Sjögren's syndrome inappropriately express major histocompatibility complex molecules, La(SSB) antigen, and heat-shock proteins. *J. Clin. Immunol.* 12: 259–265.

The American Journal of Pathology, Vol. 180, No. 5, May 2012

DOI: 10.1016/j.ajpath.2012.01.019

Cell Injury, Repair, Aging, and Apoptosis

Age-Related Dysfunction of the Lacrimal Gland and Oxidative Stress

Evidence from the Cu,Zn-Superoxide Dismutase-1 (Sod1) *Knockout Mice*

Takashi Kojima,[*†] Tais H. Wakamatsu,[*†] Murat Dogru,[*‡] Yoko Ogawa,[†] Ayako Igarashi,[‡] Osama M.A. Ibrahim,[*†] Takaaki Inaba,[†] Takahiko Shimizu,[§] Setsuko Noda,[¶] Hiroto Obata,[‖] Shigeru Nakamura,[**] Alda Wakamatsu,[††] Takuji Shirasawa,[‡‡] Jun Shimazaki,[‡] Kazuno Negishi,[†] and Kazuo Tsubota[†]

From the Departments of Ocular Surface and Visual Optics[*] and Ophthalmology,[†] Keio University School of Medicine, Tokyo, Japan; the Department of Ophthalmology,[‡] Tokyo Dental College, Chiba, Japan; the Research Team for Mechanism of Aging, Molecular Gerontology,[§] Tokyo Metropolitan Institute of Gerontology, Tokyo, Japan; the Department of Nursing,[¶] Tokai University School of Health Science, Kanagawa, Japan; the Department of Ophthalmology,[‖] Jichi Medical University School of Medicine, Tochigi, Japan; the Research Center,[**] Ophtecs Corporation, Hyogo, Japan; the Department of Pathology,[††] São Paulo University School of Medicine, São Paulo, Brazil; and the Department of Aging Control Medicine,[‡‡] Juntendo University Graduate School of Medicine, Tokyo, Japan

An imbalance between free radical generation and radical scavenging antioxidant systems results in oxidative stress, which has been associated with cell injury observed in many age-related diseases. The superoxide dismutase (SOD) family is a major antioxidant system, and deficiency of Cu,Zn-superoxide dismutase-1 (Sod1) in mice leads to many different phenotypes that resemble accelerated aging. In this study we examined the morphologic features and the secretory functions of the lacrimal glands in *Sod1*$^{-/-}$ mice. Lacrimal glands showed atrophy of acinar units; fibrosis; infiltration with CD4^{+} T cells, monocytes, and neutrophils; increased staining with both 4-hydroxy-2-nonenal and 8-hydroxy-2′-deoxyguanosine; increases in apoptotic cells; and the presence of the epithelial-mesenchymal transition in senescent *Sod1*$^{-/-}$ mice. Electron microscopy findings revealed evidence of epithelial-mesenchymal transition, presence of swollen and degenerated mitochondria, and the presence of apoptotic cell death in the lacrimal glands of senescent *Sod1*$^{-/-}$ mice. These alterations were also associated with the accumulation of secretory vesicles in acinar epithelial cells, decreased production of both stimulated and nonstimulated tears, and a decline in total protein secretion from the lacrimal glands. Our results suggest that *Sod1*$^{-/-}$ mice may be a good model system in which to study the mechanism of reactive oxygen species–mediated lacrimal gland alterations. *(Am J Pathol 2012, 180: 1879–1896; DOI: 10.1016/j.ajpath.2012.01.019)*

Aging is associated with damage to tissues by free radicals. An imbalance between generation of free radicals and radical scavenging antioxidant systems results in oxidative stress, a condition that has been associated with cell injury observed in many age-related diseases and is also considered a major factor in the process of senescence.[1] One of the well-known antioxidant defense systems is superoxide dismutase (SOD), an enzyme system that is composed of three isozymes: SOD1, SOD2, and SOD3. Among them, SOD1 is widely distributed in the tissues and represents 90% of the total SOD activity.[2,3]

Supported by research grants from Johnson and Johnson Vision Care Company and Grants-in-Aid for Scientific Research C (KAKENHI, 21592245).

Accepted for publication January 5, 2012.

T.K. and T.H.W. contributed equally to the work.

Supplemental material for this article can be found at *http://ajp.amjpathol.org* or at doi: 10.1016/j.ajpath.2012.01.019.

Address reprint requests to Murat Dogru, M.D., Ocular Surface and Visual Optics Department, Keio University School of Medicine, Shinanomachi 35, Shinjuku-ku, Tokyo 160-8582, Japan. E-mail: catherine@z8.keio.jp or muratodooru@yahoo.com.

Previously, Imamura et al[4] reported that *Sod1* gene knockout in a mouse model was associated with signs of oxidative stress–related retinal damage and features of age-related macular degeneration (AMD), an aging disease of the human retina.

The prevalence of AMD in the US population 40 years or older is estimated to be 1.47%.[5] Even more prevalent than AMD is another age-related ophthalmic disorder, the dry eye disease, the prevalence of which varies from 3.98% to 9.80% in the United States.[6] Dry eye, which is a visually disabling disease,[6] has been reported to be a major public health issue in many societies with a significant effect on quality of life and especially on the visual quality of patients with this disorder.[6]

Evidence from mouse models and human studies of dry eye disease showed decreased tear production, corneal epithelial damage, and lacrimal gland inflammation as important alterations in the pathogenesis of dry eye disease.[7–13] With the aim to investigate the eligibility of the *Sod1* knockout ($Sod1^{-/-}$) mice as a model for age-related dry eye disease, we studied the functional and histopathologic alterations of the lacrimal gland in the $Sod1^{-/-}$ mice, comparing the results with wild-type (WT) mice. We also investigated the histopathologic changes in human lacrimal gland samples obtained soon after death from young and elderly individuals.

Materials and Methods

Animals

Seventeen $Sod1^{-/-}$ male mice with C57BL/background and 14 C57BL6 strain WT male mice were examined at 10 and 50 weeks in this study. The $Sod1^{-/-}$ mice were received from the Tokyo Metropolitan Institute of Gerontology and the WT C57BL/6 mice were purchased from Japan Clea (Osaka, Japan). $Sod1^{-/-}$ mice were backcrossed to $Sod2^{flox/flox}$[14] for two generations to obtain the $Sod1^{-/-}$, $Sod2^{flox/flox}$. All studies were performed in accordance with the Association for Research in Vision and Ophthalmology Statement for the Use of Animals in Ophthalmic and Vision Research.

Aqueous Tear Production Measurements

Aqueous tear production was measured with phenol red–impregnated cotton threads (Zone-Quick, Showa Yakuhin Kako Co., Ltd., Tokyo, Japan) without anesthesia. The validity of this test in mice has been previously described.[15] The threads were held with a jeweler forceps and then immersed into the tear meniscus in the lateral canthus for 60 seconds. The length of wetting of the thread was measured in millimeters. Aqueous tear production was weight adjusted by dividing the amount of total aqueous tear produced in 60 seconds by weight. In a separate experiment to determine the incidence of dry eye disease, 40 $Sod1^{-/-}$ male mice and 118 WT male mice aged 50 weeks underwent weight and aqueous tear production measurements. To be able to define the incidence of dry eye disease in mice, we defined dry eye disease as a cotton thread test value of <0.1 mm/g and a corneal fluorescein staining score exceeding 3 points. We then calculated the percentages of mice with dry eye disease in each group.

Ocular Surface Epithelial Damage Assessment

Corneal fluorescein staining was evaluated with slit lamp biomicroscopy using cobalt blue light after instillation of 2 μL of 0.5% sodium fluorescein. Excess of fluorescein was wiped from the lateral tear meniscus. The cornea was examined with a handheld slit lamp 2 minutes after fluorescein instillation. Punctuate staining was recorded using a grading system of 0 to 3 points for superior, central, and inferior corneal areas. The fluorescein staining scores ranged from a minimum of 0 to a maximum of 9 points.

Pilocarpine-Stimulated Aqueous Tear Production Measurements

Tear secretion was stimulated 3 minutes after anesthesia (6 mg/mL of ketamine and 4 mg/mL of xyladine) by intraperitoneal injection of 0.06% pilocarpine solution (3 mg/kg; Santen Pharmaceutical Co., Ltd., Osaka, Japan), a nonselective muscarinic receptor agonist of the parasympathetic nervous system. Tears were collected from the lateral canthus for 15 minutes using 5 μL of graded capillary microglass tubes (Hirschmann Laborgerate and GmbH & Co., Eberstadt, Germany), and graticule readings were recorded at the end of each measurement.

Lacrimal Gland Carbachol–Stimulated Total Protein Secretion Measurements

The nerves in the lacrimal gland provide the major stimuli for secretion of proteins, electrolytes, and water.[16–18] To test the total protein secretion from the lacrimal glands, we exposed lacrimal gland fragments to cholinergic agonists and measured the amount of protein secreted in response to carbachol, a drug that binds and activates the acetylcholine receptor. Mice lacrimal glands were weighed before being cut into small fragments of 1 to 2 mm with a scalpel blade. The fragments were washed in 5 mL of saline solution containing 116 mmol/L NaCl, 5.4 mmol/L KCl, 1.8 mmol/L $CaCl_2$, 0.81 mmol/L $MgCl_2$, 1.01 mmol/L NaH_2PO_4, 26.2 mmol/L $NaHCO_3$, and 5.6 mmol/L dextrose (pH 7.4), maintained at 37°C and vigorously bubbled with 95% O_2 and 5% CO_2 in a beaker for 10 minutes. The solution was changed three times and discarded. The gland fragments were then incubated in 1 mL of saline for 10 minutes at 37°C, and the saline was removed and replaced with fresh medium. This cycle was repeated three times, and the saline was collected after each 10-minute incubation. The protein level measured in these samples represented the basal total protein secretion from the glands. After another 10 minutes of incubation, the medium was removed and saved, and the protein levels in these solutions represented the stimulated total protein secretion in response to carbachol. One gland was used in each experiment. The lacrimal gland samples were analyzed for total protein with a Coomassie protein assay kit (Pierce, Rockford, IL). Bovine serum

albumin was used as the standard protein, and standards were run with each assay. Protein concentrations were determined from the standard curves measured with each assay. The assays were performed in a microplate reader (model EL 808; Bio-Tek Instruments, Winooski, VT) at 595 nm. Both samples and standards were read in duplicate in 96-well flat-bottomed microplates (Costar; Corning Inc., Corning, NY). Total protein concentration was determined with the software provided by the manufacturer (KC4 version 2.7; Bio-Tek Instruments). Stimulated protein secretion was calculated by subtracting the basal protein secretion levels from the post–carbachol-stimulated protein secretion levels. The readings from the plate reader were then converted to micrograms per milliliter per minute.

Tear Fluid Collections

A total of 10 μL of 0.1 mol/L PBS was introduced onto the ocular surface by a micropipette and then collected with a 10-μL glass capillary tube (Hirschmann Laborgerate and GmbH & Co) from the lateral canthus. This procedure was performed at 10 and 50 weeks in both *Sod1*$^{-/-}$ and WT mice. Collected tears were stored at −80°C until tear cytokine concentration assessments.

Cytometric Bead Array for Assessment of Inflammatory Cytokines in Tears

The Becton Dickinson Cytometric Bead Array system was used to investigate the sensitivity of amplified fluorescence detection by flow cytometry to measure soluble analyses in particle-based immunoassay. Each bead provides a capture surface for a specific protein and is analogous to an individual coated well in an enzyme-linked immunosorbent assay (ELISA) plate. The testing allows the detection of multiple analyses in a small-volume sample. We quantitatively measured IL-6, IL-10, monocyte chemoattractant protein-1 (MCP-1), interferon (IFN)-γ, tumor necrosis factor (TNF), and IL-12p70 protein levels in tears and serum samples using the mouse inflammation kit (BD Bioscience, Franklin Lakes, NJ).

Blood was collected from the intracardiac space and centrifuged at 9100 × *g* for 5 minutes at 4°C. Serum was separated from the clotted blood and stored at −80°C. After reconstituting the mouse inflammation standards, the cytokine standard mixture (20 μL) and the tear and serum (20 μL) samples were diluted with 30 μL of the assay diluent. The standards and samples were added to a mixture of 50 μL of capture antibody-bead reagent and detector antibody-phosphatidylethanolamine phycoerythrin reagent. The mixture (150 μL) was subsequently incubated for 2 hours at room temperature and washed with 1 mL of wash buffer (from the kit) to remove unbound detector antibody-phycoerythrin reagent. After washing, the samples and standards were centrifuged at 200 × *g* for 5 minutes, and then the supernatants were carefully removed. The bead pellets were resuspended with 300 μL of wash buffer before data acquisition using flow cytometry.

Flow cytometric analysis was performed using a FACSCalibur flow cytometer (Becton Dickinson Immunocytometry Systems, San Jose, CA). Data were acquired and analyzed using the Becton Dickinson Cytometric Bead Array software version 1.4 (BD Bioscience).[19]

Lacrimal Gland Specimen Collections

Animals were sacrificed at 10 and 50 weeks. The preauricular lacrimal glands were rapidly removed by trimming the glands from the surrounding tissues. Samples were divided and fixed in 4% buffered paraformaldehyde for stainings or stored in 2.5% glutaraldehyde in 0.1M phosphate for electron microscopy or were prepared for protein secretion analysis.

Histopathologic Assessment of Lacrimal Gland Specimens

All lacrimal gland specimens were immediately fixed in 4% buffered paraformaldehyde, embedded in paraffin wax, cut into 4-μm–thick paraffin sections, and processed according to conventional histological techniques, including H&E and Mallory stainings.[20,21]

Lacrimal Gland Acinar Unit and Secretory Vesicle Density Quantifications

Five randomly selected nonoverlapping areas in each specimen in 890 × 705-μm frames were digitally photographed (Axioplan2imaging; Carl Zeiss, Jena, Germany). A total of five images from each *Sod1*$^{-/-}$ or WT mouse were taken with the photographer masked to the mouse genetic information. The acinar units and secretory vesicles were counted manually, and scores from the samples were averaged as the lacrimal acinar unit density for that lacrimal gland.

Lacrimal Gland Inflammatory Cell Density Assessment

Using an image capturing software (Adobe Photoshop Creative Suite version 8.0.1, San Jose, CA), a subset of color that indicated the stained areas (brown color) was selected from the raw pictures and analyzed using ImageJ version 1.410 (NIH, Bethesda, MD). The density of inflammatory cells in each picture was measured and expressed in pixels.[2]

IHC Staining for Oxidative Stress Markers and CD45 Panleukocyte Antigen

Lipid peroxidation was assessed by immunohistochemical (IHC) detection of 4-hydroxy-2-nonenal (4-HNE). Oxidative DNA damage was investigated by IHC staining with anti–8-hydroxy-2′-deoxyguanosine (8-OHdG) antibodies. The avidin-biotin-peroxidase complex (ABC) method was used in immunostainings. Tissues were fixed overnight in a 4% buffered paraformaldehyde solution

and processed for paraffin embedding. Sections 4 μm thick were cut from paraffin wax blocks, mounted on precoated glass slides, deparaffinized, and rehydrated. To block nonspecific background staining, lacrimal gland sections were treated with normal horse serum (Vector Laboratories, Burlingame, CA) for 2 hours at room temperature. The tissues were then treated with mouse anti–8-OHdG monoclonal antibody at a concentration of 10 μg/mL diluted with horse-blocking serum (Japan Institute for the Control of Aging, Shizuoka, Japan) and anti–4-HNE monoclonal antibody at a concentration of 25 μg/mL diluted with horse-blocking serum (Japan Institute for the Control of Aging) for 2 hours at room temperature. For the negative controls, the primary antibody was replaced with mouse IgG1 Isotype control (MOPC-21; Sigma, St. Louis, MO). Endogenous peroxidase activity was blocked using 3.0% H_2O_2 in methanol for 3 minutes. The sections were incubated for 30 minutes with biotin-labeled horse anti-mouse IgG serum (Vector Laboratories), followed by avidin-biotin-alkaline phosphatase complex treatment (Vector Laboratories) for 30 minutes. The sections were washed in PBS buffer, developed in 3,–3′-diaminobenzidine (DAB) chromogen solution (Vector Laboratories), lightly counterstained with hematoxylin for 4 minutes at room temperature, washed with tap water, dehydrated, and mounted. For CD45 IHC stainings, we used the purified anti-mouse CD45 antibody solution diluted with rabbit blocking serum at a concentration of 10 μg/mL (BioLegend, San Diego, CA) and the peroxidase system Vectastain ABC kit (rat IgG; Vector Laboratories). To block nonspecific background staining, lacrimal gland sections were treated with normal rabbit serum (Vector Laboratories) for 2 hours at room temperature. The tissues were then treated with 10 μg/mL of anti-mouse CD45 for 2 hours at room temperature. For the negative controls, the primary antibody was replaced with rat IgG2B isotype control at the same concentration of the primary antibody (R&D Systems, Minneapolis, MN). Endogenous peroxidase activity was blocked using 3.0% H_2O_2 in methanol for 3 minutes. The sections were incubated for 30 minutes with biotin-labeled rabbit anti-rat IgG serum (Vector Laboratories), followed by avidin-biotin-alkaline phosphatase complex treatment (Vector Laboratories) for 30 minutes. The sections were washed in 0.1M PBS, developed in prepared DAB chromogen solution (Vector Laboratories), lightly counterstained with hematoxylin for 4 minutes at room temperature, washed with tap water, dehydrated, and mounted.

Fluorescent IHC Staining for EMT Markers and Inflammatory Cell Markers

Epithelial mesenchymal transition (EMT) has been reported to play a crucial role in fibrosis of tissues.[22,23] To evaluate whether EMT is involved in the pathogenesis of fibrosis in aged *SOD1*$^{-/-}$ mice, mice lacrimal gland specimens were immunostained with epithelial cell marker (E-cadherin) and mesenchymal cell marker [α-smooth muscle actin (SMA)]. To evaluate the continuity of basement membrane in acinar units, type I collagen was immunostained. IHC for EMT markers was performed as described previously.[24]

To differentiate the type of inflammatory cells in the lacrimal gland, specimens were immunostained with CD4, CD11b, and Gr-1 antibodies. Fluorescent IHC was performed as follows. Briefly, cryosections (6 μm) from mouse lacrimal gland were fixed in 4% paraformaldehyde for 20 minutes. After blocking with 1% bovine serum albumin PBS containing 2% donkey serum, sections were incubated overnight with primary antibodies. After washing with PBS, the sections were incubated for 30 minutes with secondary antibodies and observed using a fluorescence microscope (Carl Zeiss, Oberkochen, Germany). For negative control, isotype control IgG was applied instead of primary antibody. The specimens were immunostained with the following primary antibodies: rabbit anti–α-SMA antibody (0.01 mg/mL, ab5694; Abcam, Boston, MA), rat anti–E-cadherin antibody (0.01 mg/mL, ab11512; Abcam), rabbit antitype I collagen antibody (0.01 mg/mL, ab292; Abcam), rat anti-CD4 antibody (0.01 mg/mL, 14–0041; eBioscience, San Diego, CA), rat anti-CD11b (0.026 mg/mL, ab8878; Abcam), and rat anti–Gr-1 (0.01 mg/mL, ab25377; Abcam). The secondary antibodies were fluorescein isothiocyanate–conjugated anti-rabbit IgG antibody (0.0075 mg/mL; Jackson Immunoresearch Laboratories, West Grove, PA) and fluorescein isothiocyanate–conjugated anti-rat IgG antibody (0.0075 mg/mL; Jackson Immunoresearch Laboratories). DAPI (Vector Laboratories) was used for nuclear staining.

Immunofluorescence Staining for Apoptosis Markers

Terminal deoxyribonucleotidyl transferase–mediated deoxyuridine triphosphate digoxigenin nick end labeling (TUNEL) staining was performed using the *in situ* Cell Death Detection Kit, TMR Red (Roche Applied Science, Mannheim, Germany). Initially, 10 μg/mL of proteinase K (Roche Applied Science) in 10 mmol/L Tris/HCl (pH 7.4) was applied to the lacrimal gland specimens and left for 15 minutes at room temperature. After washing the samples with 0.1M PBS twice, TUNEL reaction mixture (Roche Applied Science) was added to the samples and the label solution on the negative control sample, which were then incubated at 37°C for 60 minutes in a dark room. The specimens were rinsed in 1M PBS for 5 minutes three times, and then 100 μL of 0.5 μg/mL of DAPI diluted in Tris-buffered saline and Tween-20 was added on samples for 5 minutes at room temperature. Finally, the specimens were washed with 1M PBS and mounted with aqueous mounting medium Permafluor (Beckman Coulter, Marseille, France). Caspase-3 immunofluorescent staining was performed using the Alexa Fluor 488 Goat Anti-Rabbit SFX Kit (Molecular Probes, Eugene, OR). The samples were initially blocked with four drops of Image-iT FX signal enhancer (Molecular Probes) for 30 minutes and then with 10% normal goat serum (Dako, Tokyo, Japan) diluted in Block-Ace solution (dilution factor 1:25 in 0.1M PBS) for 2 hours. Primary cleaved caspase-3 antibody (dilution factor 1:200; Cell Signaling,

Danvers, MA) was added on the specimens, which were kept refrigerated overnight at 4°C. Subsequently, after wash with 0.1M PBS, the secondary antibody anti-IgG Alexa 488 (dilution 1:200; Molecular Probes) was applied for 45 minutes in a dark incubation chamber. After wash with 0.1M PBS, specimens were coverslipped with fluorescent mounting medium with DAPI (Vectashield; Vector Laboratories). Sections were examined and photographed with an epifluorescence microscope (Axioplan2imaging; Carl Zeiss).

Transmission Electron Microscopy Examination

Lacrimal gland specimens were immediately fixed with 2.5% glutaraldehyde in 0.1M PBS (pH 7.4) immersed for 4 hours at 4°C, and then washed three times with 0.1M PBS solution. The samples were then postfixed in 2% osmium tetroxide, dehydrated in a series of ethanol and propylene oxide, and embedded in epoxy resin. One-micrometer sections were stained with methylene blue, and the lacrimal gland tissues were thin sectioned on an Ultratome (LKB, Gaithersburg, MD) with a diamond knife. Sections were collected on 150-mesh grids, stained with uranyl acetate and lead citrate, examined, and photographed using an electron microscope (model 1200 EXII; JEOL, Tokyo, Japan).

Serum 8-OHdG Concentrations Assessed by ELISA

A commercially available 8-OHdG ELISA kit (Japan Institute for the Control of Aging) was used to determine the serum 8-OHdG concentration, as reported previously.[25] A total of 200 μL of serum was used for 8-OHDG measurements.

Lacrimal Gland IHC Staining for Oxidative Stress and Inflammatory Cell Markers in Humans

Postmortem human lacrimal gland tissues from 6 individuals 17 to 48 years old (the young group) and 6 individuals 76 to 87 years old (the old group) were donated by Dr. Hiroto Obata. The samples were studied under institutional review board permission at Keio University School of Medicine. All lacrimal gland specimens were immediately fixed in 4% buffered paraformaldehyde, embedded in paraffin wax, cut into 4-μm–thick paraffin sections, and processed according to conventional histologic techniques, including H&E and Mallory staining fibrosis. Oxidative stress–induced lipid peroxidation was assessed by IHC detection of 4-HNE protein adducts. Oxidative DNA damage was investigated by IHC staining of 8-OHdG. The presence of inflammatory cells was investigated by IHC using anti-CD45 antibodies (concentration: 0.01 mg/mL; Dako, Glostrup, Denmark). The ABC method was used for immunostaining. Antigen retrieval was achieved by microwaving in 10 mmol/L sodium citrate buffer for 5 minutes then cooling for 20 minutes. The tissues were then treated with mouse anti–8-OHdG monoclonal antibody at a concentration of 10 μg/mL diluted with horse-blocking serum (Japan Institute for the Control of Aging) and anti–4-HNE monoclonal antibody at a concentration of 25 μg/mL diluted with horse-blocking serum (Japan Institute for the Control of Aging) for 2 hours at room temperature. For the negative controls, the primary antibody was replaced with mouse IgG1 isotype control (MOPC-21; Sigma). Endogenous peroxidase activity was blocked using 3.0% H_2O_2 in methanol for 3 minutes. The sections were incubated for 30 minutes with biotin-labeled horse anti-mouse IgG serum (Vector Laboratories), followed by avidin-biotin-alkaline phosphatase complex treatment (Vector Laboratories) for 30 minutes. The sections were washed in PBS buffer, developed in prepared DAB chromogen solution (Vector Laboratories), lightly counterstained with hematoxylin for 4 minutes at room temperature (4-HNE stainings), washed with tap water, dehydrated, and mounted.

Quantitative RT-PCR for EMT Markers

Mouse lacrimal glands were preserved overnight in RNA later (Applied Biosystems, Carlsbad, CA) after prompt excision. Tissues were then transferred into isogen (Nippon Gene, Tokyo, Japan) and homogenized well. Total RNA was extracted, cleaned up, and treated with DNase using RNeasy mini kit (Qiagen, Valencia, CA). cDNA synthesis was performed using iScript cDNA Synthesis Kit (Bio-Rad, Hercules, CA). SYBR Green–based quantitative real-time PCR was performed using StepOnePlus system (Applied Biosystems). Mouse glyceraldehyde-3-phosphate (GAPDH) (sense 5′-TGACGTGCCGCCTGGAGAAA-3′, antisense, -3′AGTGTAGCCCAAGATGCCCTTCAG5′-), Snail (sense 5′-TGGAAAGGCCTTCTCTAGGC-3′, antisense, -3′CTTCACATCCGAGTGGGTTT5′-), E-cadherin (sense 5′-GGCTTCAGTTCCGAGGTCTA-3′, antisense, -3′CGAAAA-GAAGGCTGTCCTTG5′-), α-SMA (sense 5′-CTGACAGAG-GCACCACTGAA-3′, antisense, -3′AGAGGCATAGAGGG-ACAGCA5′-) primers were used as templates for GAPDH, Snail, E-cadherin, and α-SMA amplification. Data were normalized to GAPDH.

Results

Lack of SOD1 Accelerates Oxidative Lipid and DNA Damage in the Lacrimal Glands and Causes Elevation of Serum 8-OHdG Levels

Aldehyde molecules generated endogenously during the process of lipid peroxidation have been reported to be associated with oxidative stress in cells and tissues.[26] 4-HNE is one of the best recognized and most studied cytotoxic product of lipid peroxidation.[26]

To evaluate the influence of the *Sod1* knockout on the lipid peroxidation process, we initially performed lacrimal gland IHC stainings with anti–4-HNE antibodies (Figure 1A). Specimens from 50-week-old *Sod1*$^{-/-}$ mice exclusively showed dense staining compared with the specimens from the WT mice at 10 and 50 weeks and *Sod1*$^{-/-}$ mice at 10 weeks (Figure 1A). The mean areas (pixels^2) of positively stained cells were 11.98 ± 4.26 for WT mice

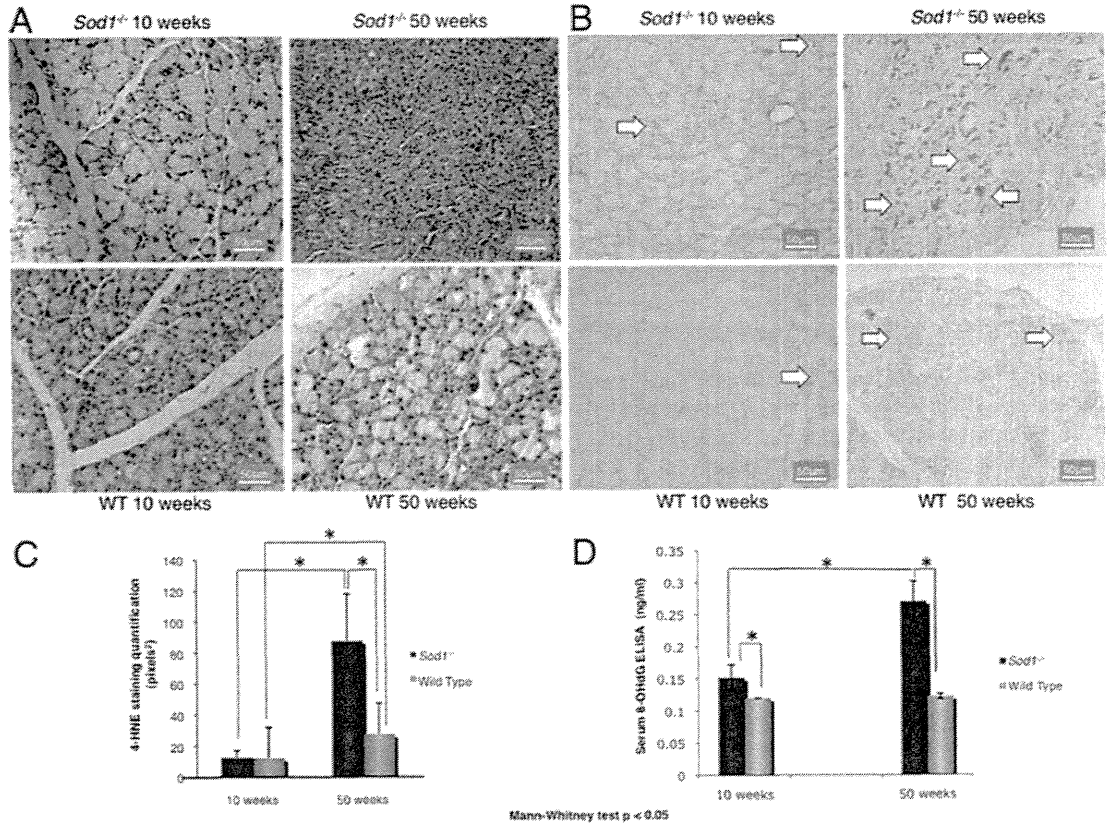

Figure 1. Oxidative lipid and DNA changes in the lacrimal glands and alterations in serum 8-OHdG levels. **A:** Late-phase lipid peroxidation marker 4-HNE stained cells positively, showing a dense staining in the 50-week-old *Sod1*$^{-/-}$ mouse. WT mice specimens were also stained but not to the extent observed in *Sod1*$^{-/-}$ mice. **B:** Acinar cell nuclei showed scanty staining with 8-OHdG antibodies in the *Sod1*$^{-/-}$ and WT mice at 10 weeks. There was a marked increase in nuclear staining from 10 to 50 weeks, exclusively in all *Sod1*$^{-/-}$ mice. Relatively more acinar cellular nuclei stained with anti–8-OHdG antibodies in the *Sod1*$^{-/-}$ mice at 50 weeks compared with lacrimal gland specimens from WT mice at 50 weeks. **C:** Semiquantitative analysis of the extent of cellular staining for 4-HNE revealed a statistically significance increase in the 50-week-old mice group compared with the 10-week-old group and a significant elevation in staining for the *Sod1*$^{-/-}$ mice group compared with the WT mice at 50 weeks ($P < 0.0001$). Error bars indicate SD from at least five independent samples. **D:** The mean 8-OHdG serum concentrations were significantly higher in the *Sod1*$^{-/-}$ than the WT mice at 10 ($P < 0.05$) and 50 weeks ($P = 0.008$). Note the significant elevation of serum 8-OHdG concentration from 10 to 50 weeks in the *Sod1*$^{-/-}$ mice. Error bars indicate SD from at least five independent samples per group of two separate experiments.

at 10 weeks, 12.29 ± 4.64 for *Sod1*$^{-/-}$ mice at 10 weeks, 27.23 ± 12.37 for WT mice at 50 weeks, and 87.43 ± 30.37 for *Sod1*$^{-/-}$ mice at 50 weeks. The extent of lacrimal gland staining with 4-HNE antibodies showed a significant increase ($P < 0.0001$) in both *Sod1*$^{-/-}$ and WT mice from 10 weeks to 50 weeks as shown in Figure 1C. The extent of staining with 4-HNE antibodies in the *Sod1*$^{-/-}$ mice at 50 weeks was significantly higher ($P < 0.0001$) than the WT mice at 50 weeks (Figure 1C).

8-OHdG is a well-known marker for oxidative stress–induced DNA damage.[26] To assess the cellular DNA damage, we next performed IHC with anti–8-OHdG antibodies. Acinar cell nuclei showed scanty staining with 8-OHdG antibodies in the *Sod1*$^{-/-}$ and WT mice at 10 weeks. There was a marked increase in nuclear staining from 10 to 50 weeks in all *Sod1*$^{-/-}$ mice. Relatively more acinar cellular nuclei stained with anti–8-OHdG antibodies in the *Sod1*$^{-/-}$ mice at 50 weeks compared with lacrimal gland specimens from WT mice at 50 weeks (Figure 1B). Serum 8-OHdG assessment has been shown to be a reliable marker for elevated systemic oxidative stress status.[26] To investigate this possibility, we performed ELISA to determine serum 8-OHdG concentrations in the *Sod1*$^{-/-}$ and WT mice at both 10 and 50 weeks. The mean 8-OHdG concentrations were significantly higher in the *Sod1*$^{-/-}$ than the WT mice at 10 ($P < 0.05$) and 50 weeks ($P = 0.008$).

A significant timewise increase was seen in the mean serum 8-OHdG concentration in the *Sod1*$^{-/-}$ mice from 10 to 50 weeks. The mean values for serum 8-OHdG concentrations were 0.12 ± 0.01 ng/mL for WT mice at 10 weeks, 0.15 ± 0.02 ng/mL for *Sod1*$^{-/-}$ mice at 10 weeks, 0.12 ± 0.01 ng/mL for WT mice at 50 weeks, and 0.27 ± 0.03 ng/mL for *Sod1*$^{-/-}$ mice at 50 weeks (Figure 1D).

Oxidative Lipid and DNA Damage Is Associated with Ultrastructural Mitochondrial Alterations

At organelle level, we could observe, by transmission electron microscopy examination, certain ultrastructural changes in the mitochondria, which are the power houses of the living cells.[27] Whereas the mitochondria did not show any phenotypic alterations from 10 to 50

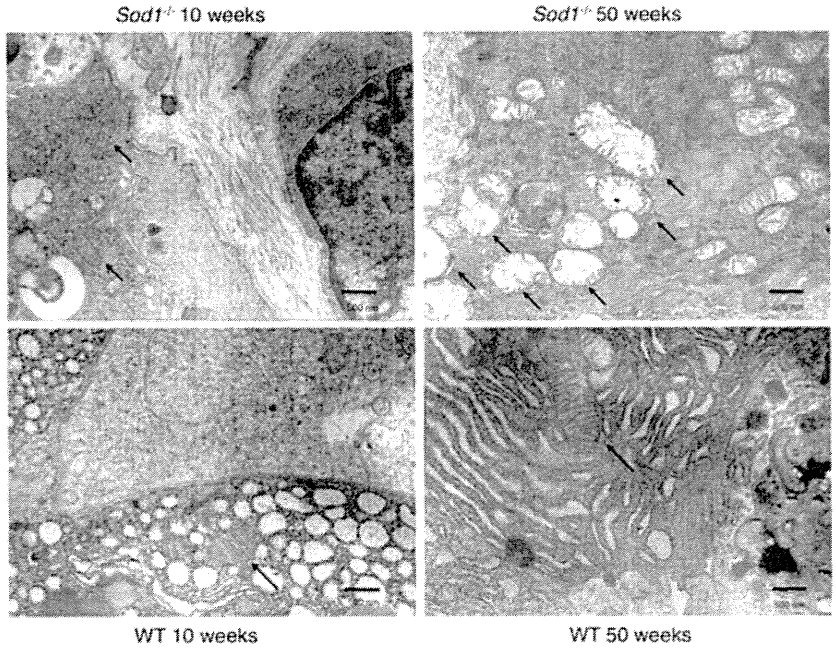

Figure 2. Ultrastructural mitochondrial alterations. Transmission electron microscopic examination of WT and *Sod1*$^{-/-}$ mice at 10 and 50 weeks revealed marked ultrastructural changes in the mitochondria. Whereas the mitochondria did not show any phenotypic alterations from 10 to 50 weeks in the WT mice, mitochondrial swelling, disorientation, shortening, and disorganization of cristae were noted at 50 weeks in the *Sod1*$^{-/-}$ mice.

weeks in the WT or the *Sod1*$^{-/-}$ mice at 10 weeks, mitochondrial swelling, disorientation, shortening, and disorganization of cristae were noted prominently at 50 weeks in 88.2% of the *Sod1*$^{-/-}$ mice (Figure 2).

Sod1 *Knockout Is Also Associated with Increased Inflammatory Response in the Lacrimal Gland and Elevation of Inflammatory Cytokines in Tears and Serum*

Oxidative damage has been reported to be associated with induction of inflammation.[28–30] To check whether the aforementioned oxidative stress changes were associated with increased lacrimal gland inflammation, we performed IHC stainings with CD45 antibodies. CD45 is a panleukocyte marker and has been shown to be a good marker for staining of T lymphocytes, B lymphocytes, granulocytes, monocytes, and macrophages.[31] Whereas specimens from the 10-week-old *Sod1*$^{-/-}$ and WT mice showed scanty staining of inflammatory cells with anti-CD45 antibodies, there was intense staining in all specimens from the *Sod1*$^{-/-}$ mice at 50 weeks, where inflammatory cell infiltrates around glandular ducts and several foci of inflammation could be observed. Relatively more inflammatory infiltrates were observed in specimens from the 50-week-old *Sod1*$^{-/-}$ mice compared with the WT mice (Figure 3A). To differentiate the type of inflammatory cells in the 50-week-old *Sod1*$^{-/-}$ mice, we performed further IHC stainings with CD4, CD11b, and Gr-1 antibodies. CD4 is a marker of helper T cells, whereas CD11b and Gr-1 are markers for neutrophils and monocytes, respectively.

Using the ImageJ and Adobe Photoshop computer software, we quantified the total inflammatory cell counts in each specimen. The mean CD45^{+} inflammatory cell density showed a significant timewise increase from 10 to 50 weeks in both the *Sod1*$^{-/-}$ and WT mice ($P < 0.0001$ and $P = 0.0031$, respectively). The mean inflammatory cell density was significantly higher in the *Sod1*$^{-/-}$ mice at 50 weeks compared with the WT mice ($P < 0.05$) (Figure 3B). The mean CD4-, CD11b-, and Gr-1–positive inflammatory cell densities were significantly higher in the *Sod1*$^{-/-}$ mice compared with the WT mice at 50 weeks. The mean CD4-positive cell density was significantly higher than the density of other inflammatory cells in the *Sod1*$^{-/-}$ mice at 50 weeks (Figure 3B).

To investigate the inflammatory cytokine alterations in the serum and tears, we performed Cytometric Bead Array evaluating the changes in six cytokines, including IL-6, IL-10, IFN-γ, TNF-α, MCP-1, and IL-12p70. Among them, the mean serum IL-6 concentration in the *Sod1*$^{-/-}$ mice showed a significant ($P = 0.009$) timewise increase from 10 to 50 weeks (9.96 ± 12.95 pg/mL to 33.62 ± 14.98 pg/mL). The mean serum TNF-α levels were also significantly higher ($P = 0.009$) in the *Sod1*$^{-/-}$ mice (10.89 ± 3.23 pg/mL) compared with the WT mice at 50 weeks (5.6 ± 3.73 pg/mL). There was a significant ($P = 0.016$) timewise increase in the mean TNF-α serum concentration from 10 (5.13 ± 6.39 pg/mL) to 50 (10.89 ± 3.23 pg/mL) weeks in the *Sod1*$^{-/-}$ mice (Figure 3C).

The mean tear IL-6 concentration also showed a significant increase in the *Sod1*$^{-/-}$ mice from 10 to 50 weeks ($P = 0.002$). The IL-6 concentration was significantly higher ($P = 0.028$) in the *Sod1*$^{-/-}$ at 50 weeks (36.88 ± 29.23 pg/mL) compared with the WT mice at 50 weeks (14.08 ± 11.65 pg/mL). The mean tear TNF-α concentration increased significantly from 10 to 50 weeks in both the *Sod1*$^{-/-}$ (9.96 ± 12.95 pg/mL and 33.62 ± 14.98 pg/mL, respectively) and the WT mice (6.82 ± 10.38 pg/mL and 46.11 ± 17.86 pg/mL, respectively). The mean tear TNF-α concentration was significantly higher in

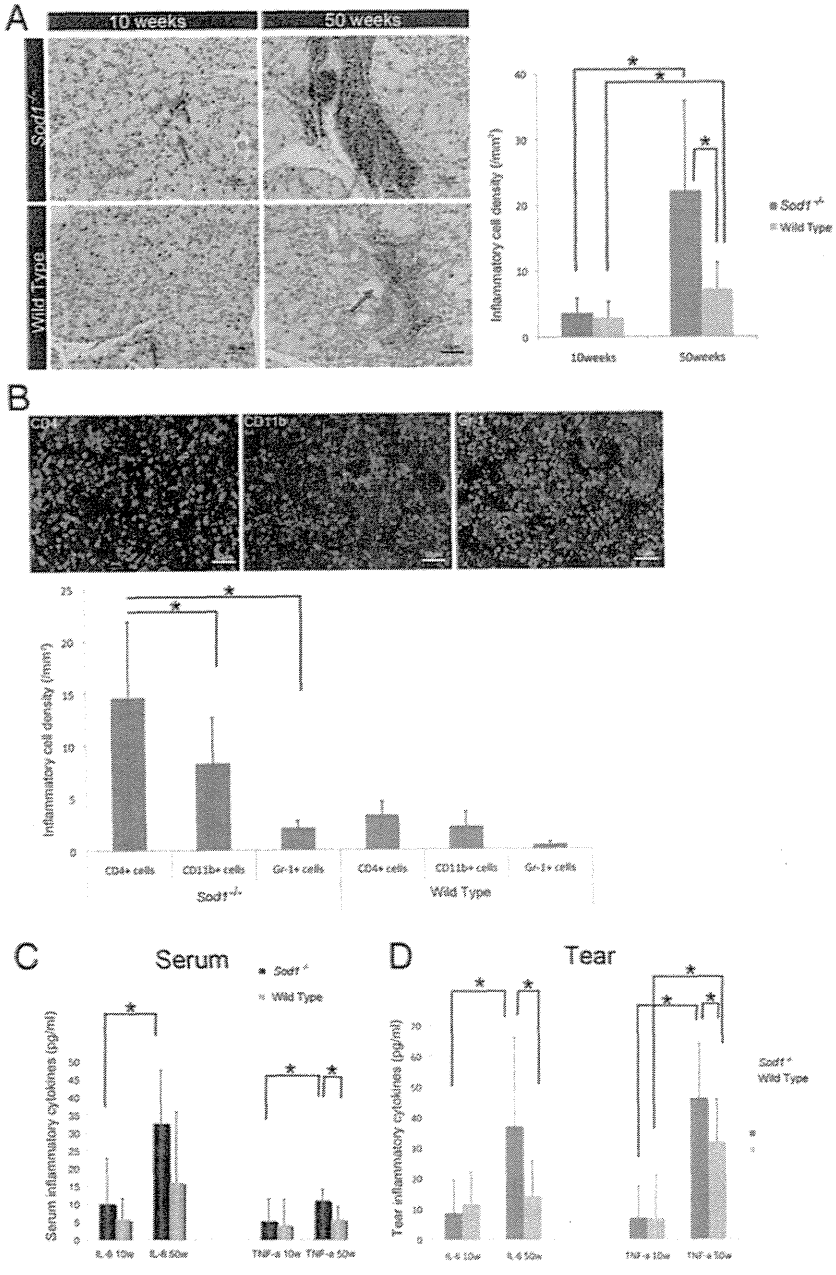

Figure 3. Inflammatory lacrimal gland, serum, and tear alterations in the $Sod1^{-/-}$ and WT mice. **A:** Specimens stained with CD45 in the 10-week-old $Sod1^{-/-}$ and WT mice showed scanty inflammatory cells. Note the relatively more intense staining in the specimen from the $Sod1^{-/-}$ mice at 50 weeks compared with the WT mice. The mean inflammatory cell densities showed a significant timewise increase from 10 weeks to 50 weeks in both the $Sod1^{-/-}$ and WT mice ($P < 0.0001$ and $P = 0.0031$, respectively). Note the significantly higher inflammatory cell density in the $Sod1^{-/-}$ mice at 50 weeks compared with the WT mice ($P < 0.05$). **B:** Specimens from the 50-week-old $Sod1^{-/-}$ mice were stained with anti-CD4, CD11b, and Gr-1 antibodies. Note the CD4-positive cells were dominant among inflammatory cells. The CD4-positive cell density (lower panel) was significantly higher than either the CD11b- or Gr-1–positive cell density. **C:** The mean serum IL-6 concentration in the $Sod1^{-/-}$ mice showed a significant ($P = 0.009$) timewise increase from 10 to 50 weeks. Serum TNF-α levels were also significantly higher ($P = 0.009$) in the $Sod1^{-/-}$ mice at 50 weeks compared with the WT mice at 50 weeks. A significant ($P = 0.016$) timewise increase was seen in the mean TNF-α serum concentration from 10 to 50 weeks in the $Sod1^{-/-}$ mice. **D:** The mean tear IL-6 concentration also showed a significant increase in the $Sod1^{-/-}$ mice from 10 to 50 weeks ($P = 0.002$). Note the significantly higher IL-6 concentration ($P = 0.028$) in the $Sod1^{-/-}$ mice at 50 weeks compared with the WT mice at 50 weeks. The mean tear TNF-α concentrations increased significantly from 10 to 50 weeks in both the $Sod1^{-/-}$ and the WT mice. Note also the significantly higher TNF-α concentration in the $Sod1^{-/-}$ mice compared with the WT mice at 50 weeks ($P < 0.05$). Error bars indicate SD from at least five independent samples per group of three separate experiments. *$P < 0.05$.

the $Sod1^{-/-}$ mice compared with the WT mice at 50 weeks ($P < 0.05$) (Figure 3D).

The mean tear IL-10, IFN-γ, MCP-1, and IL-12p70 levels did not show significant differences from 10 to 50 weeks in both the $Sod1^{-/-}$ and WT mice. There were also no significant differences in the mean IL-10, IFN-γ, MCP-1, and IL-12p70 concentrations between the WT and the $Sod1^{-/-}$ mice at 50 weeks (data not shown).

IHC and Ultrastructural Evidence of Increased Apoptosis in the Lacrimal Glands

Inflammation in the lacrimal gland has previously been shown to be associated with apoptosis in acinar cells of the lacrimal glands in dry eyes associated with Sjögren syndrome.[32,33] To investigate whether elevated oxidative damage and inflammation status were associated with increased cell death in the lacrimal glands of the current mouse model, we performed immunofluorescence staining with TUNEL and caspase-3 antibodies. TUNEL assay has been used to detect the DNA breakpoints and assess apoptotic cells.[34] Lacrimal gland samples from all $Sod1^{-/-}$ mice at 50 weeks showed marked positive staining with TUNEL for apoptotic cells (572.21 cells/mm^2) compared with specimens from $Sod1^{-/-}$ mice at 10 weeks (110.05 cells/mm^2) and WT mice at 50 weeks (247.21 cells/mm^2). Increased positive staining was also observed for the WT mice lacrimal gland specimens from

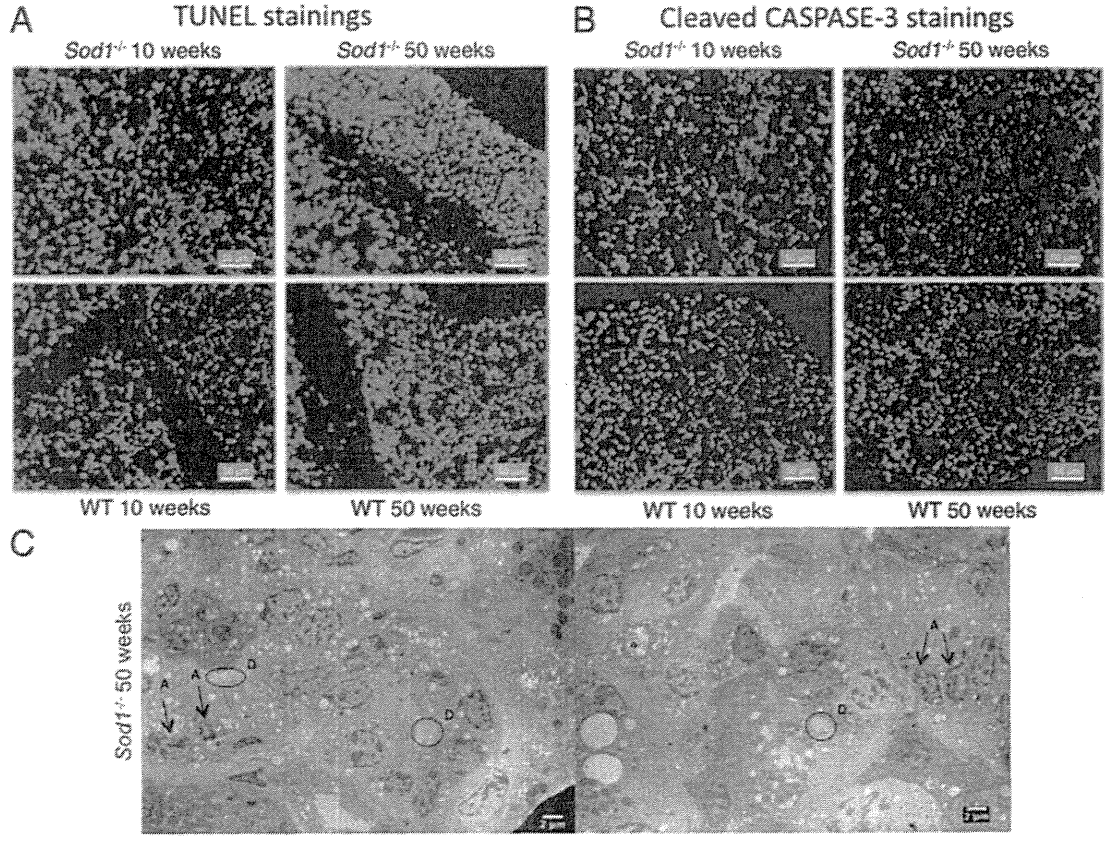

Figure 4. IHC and ultrastructural evidence of apoptosis in the lacrimal glands. **A:** Lacrimal gland samples from all *Sod1*$^{-/-}$ mice at 50 weeks showed marked positive staining with TUNEL for apoptotic cells (572.21 cells/mm^2) compared with specimens from *Sod1*$^{-/-}$ mice at 10 weeks (110.05 cells/mm^2) and WT mice at 50 weeks (247.21 cells/mm^2). Increased positive staining was also observed for the WT mice lacrimal gland specimens from 10 weeks (27.11 cells/mm^2) to 50 weeks (247.21 cells/mm^2). **B:** Specimens from the *Sod1*$^{-/-}$ mice at 50 weeks displayed relatively more positive staining (178.63 cells/mm^2) with caspase-3 antibodies for apoptotic cells compared with specimens from *Sod1*$^{-/-}$ mice at 10 weeks (65.39 cells/mm^2) and WT at 50 weeks (116.43 cells/mm^2). **C:** Note the evidence for apoptosis (**A**; **arrows**) in acinar epithelial cells by transmission electron microscopy. Specimens from the *Sod1*$^{-/-}$ mice at 50 weeks exclusively and prominently displayed fragmentation and shrinkage of the nuclei, cytoplasmic vacuole formation, and loss of nuclear membranes. The areas indicated by circles and ellipses correspond to the lacrimal gland acinar ducts (D). Images are representatives of at least five independent samples per group.

10 weeks (27.11 cells/mm^2) to 50 weeks (247.21 cells/mm^2) (Figure 4A). We also performed cleaved caspase-3 staining by immunofluorescence. Caspase-3 has been regarded to be an important mediator of apoptosis.[35] Specimens from the *Sod1*$^{-/-}$ mice at 50 weeks displayed relatively more positive staining (178.63 cells/mm^2) with caspase-3 antibodies for apoptotic cells compared with specimens from *Sod1*$^{-/-}$ mice at 10 weeks (65.39 cells/mm^2) and WT mice at 50 weeks (116.43 cells/mm^2) (Figure 4B). We also sought for evidence of apoptosis in acinar epithelial cells by transmission electron microscopy. A total of 88.2% of the specimens from the *Sod1*$^{-/-}$ mice at 50 weeks displayed marked fragmentation and shrinkage of the nuclei, cytoplasmic vacuole formation, and loss of nuclear membranes (Figure 4C). Such changes were not observed in specimens of WT mice at 10 and 50 weeks and *Sod1*$^{-/-}$ mice at 10 weeks (data not shown).

Lacrimal Gland Fibrosis and Related Morphologic Alterations in the Sod1$^{-/-}$ *and WT Mice*

As shown in Figure 5A, lacrimal glands removed from the 10-week-old WT and *Sod1*$^{-/-}$ mice showed normal ductal and acinar cell morphologic features and lobular architecture separated by interlobular connective tissue. At 50 weeks, lacrimal glands in the *Sod1*$^{-/-}$ mice exclusively developed a severe inflammatory response with inflammatory cells invading the interlobular spaces surrounding both acinar and ductal cells. Lobular atrophy due to atrophy of the acinar cells, interlobular and periductal fibrosis, and interlobular duct dilatation were observed. Slight periductal and interlobular fibrosis together with a few inflammatory cells were also noted in the WT mice lacrimal gland specimens. To further describe the extent of fibrosis, Mallory staining was performed, which stains areas of fibrosis with a dark blue color.[20,21] Almost no interlobular fibrosis was observed in both *Sod1*$^{-/-}$ and WT mice at 10 weeks. Extensive interlobular and periacinar Mallory staining was observed in the lacrimal gland specimens of all *Sod1*$^{-/-}$ mice at 50 weeks, with some slight interlobular positive staining observed in the age-matched WT mice (Figure 5B).

To quantify the lacrimal gland acinar unit densities, we counted the number of acinar units within a fixed area for all samples. We observed that there were no statistically significant differences between the mean acinar unit densities

of *Sod1*$^{-/-}$ (780.89 ± 150.05 units/μm^2) and WT (794.39 ± 78.75 units/μm^2) mice at 10 weeks. There was a decrease in the mean acinar unit densities from 10 weeks to 50 weeks in both *Sod1*$^{-/-}$ and WT mice (Figure 5C). The mean acinar unit density in the lacrimal gland specimens of the *Sod1*$^{-/-}$ mice at 50 weeks (379.72 ± 92.78 units/μm^2) was significant lower than the acinar unit density in the WT mice at 50 weeks (514.58 ± 47.43 units/μm^2) ($P < 0.001$).

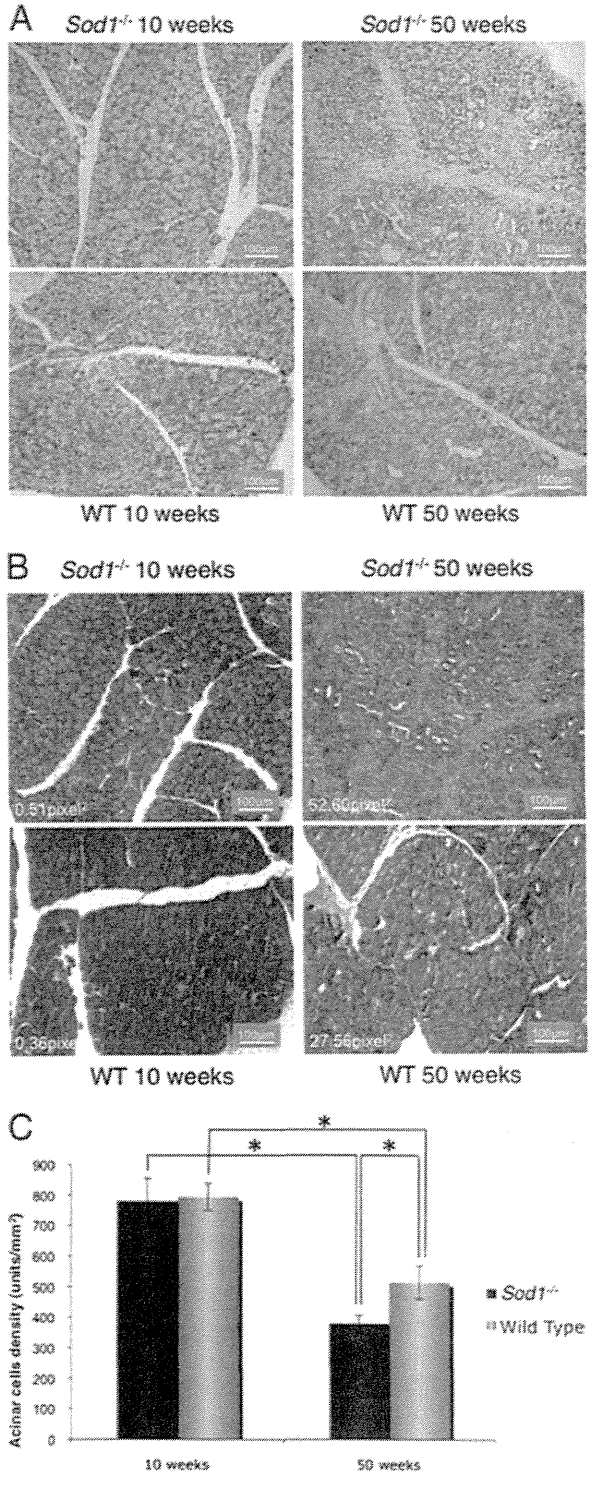

Evaluation of EMT in Lacrimal Glands of Sod1$^{-/-}$ *and WT Mice*

To further study the processes involved in lacrimal gland fibrosis, we decided to investigate the presence of EMT in the lacrimal gland. Lacrimal gland specimens were immunostained with epithelial and mesenchymal markers, namely, E-cadherin and α-SMA. Type I collagen was expressed in basement membranes of acinar cells in both *Sod1*$^{-/-}$ and WT mice (Figure 6, A–D). In eyes of 50-week-old *Sod1*$^{-/-}$ mice, disruption of basement membrane was observed (Figure 6D). α-SMA immunostaining was observed in the periacinar areas of the epithelial cells in all specimens (Figure 6, E–H). The number of α-SMA–positive cells was significantly higher in the 50-week-old *Sod1*$^{-/-}$ mice compared with the WT mice. On the other hand, positive E-cadherin staining was observed in the intercellular junctions between adjacent lacrimal gland acinar cells (Figure 6, I–L), and expression was lower in the 50-week-old *Sod1*$^{-/-}$ mice compared with the WT mice (Figure 6L). To further quantify the mRNA expression levels of EMT-related markers, SYBR Green–based quantitative real-time PCR was performed. The expression of Snail, which is an inducer of EMT, was significantly higher in the 50-week-old *Sod1*$^{-/-}$ mice than in 50-week-old WT and 10-week-old *Sod1*$^{-/-}$ mice (Figure 6M). The expression of α-SMA, which is a mesenchymal cell marker, was significantly higher in the 50-week-old *Sod1*$^{-/-}$ mice than in 50-week-old WT mice (Figure 6N). The expression of E-cadherin, which is an epithelial cell marker, was significantly lower in the 50-week-old *Sod1*$^{-/-}$ mice than the 50-week-old WT mice, the 10-week-old *Sod1*$^{-/-}$ mice, and the 10-week-old WT mice (Figure 6O). The expression level of the α-SMA/E-cadherin ratio was significantly higher in the 50-week-old *Sod1*$^{-/-}$ mice than the 50-week-old WT mice, 10-week-old *Sod1*$^{-/-}$ mice, and 10-week-old WT mice (Figure 6P).

Figure 5. Evidence of further morphologic alterations in the *Sod1*$^{-/-}$ and WT mice lacrimal glands. **A:** Lacrimal glands from the 10-week-old WT and *Sod1*$^{-/-}$ mice showed normal ductal and acinar cell morphologic features. At 50 weeks, lacrimal glands in the *Sod1*$^{-/-}$ mice exclusively developed a severe inflammatory response, with inflammatory cells invading the interlobular spaces surrounding both the acinar and ductal cells. Lobular atrophy due to atrophy of the acinar cells, interlobular and periductal fibrosis, and interlobular duct dilatations were observed. Slight periductal and interlobular fibrosis together with a few inflammatory cells were also noted in the WT mice lacrimal gland specimens. **B:** Extensive interlobular and periacinar fibrosis was observed in the lacrimal gland specimens of all *Sod1*$^{-/-}$ mice at 50 weeks, with some slight interlobular positive staining in the age-matched WT mice. Images in **A** and **B** are representatives of at least five independent samples per group. **C:** No statistically significant differences were found between the mean acinar unit densities of the *Sod1*$^{-/-}$ and WT mice at 10 weeks. There was a timewise decrease in the mean acinar unit densities from 10 weeks to 50 weeks in both *Sod1*$^{-/-}$ and WT mice ($P < 0.0001$). The mean acinar unit density in the lacrimal gland specimens of the *Sod1*$^{-/-}$ mice at 50 weeks was significant lower then the acinar unit density in the WT mice at 50 weeks (*$P < 0.001$, Mann-Whitney test). Data in **C** represents the mean and SD of combined data from seven mice per group and are representative of three separate experiments.

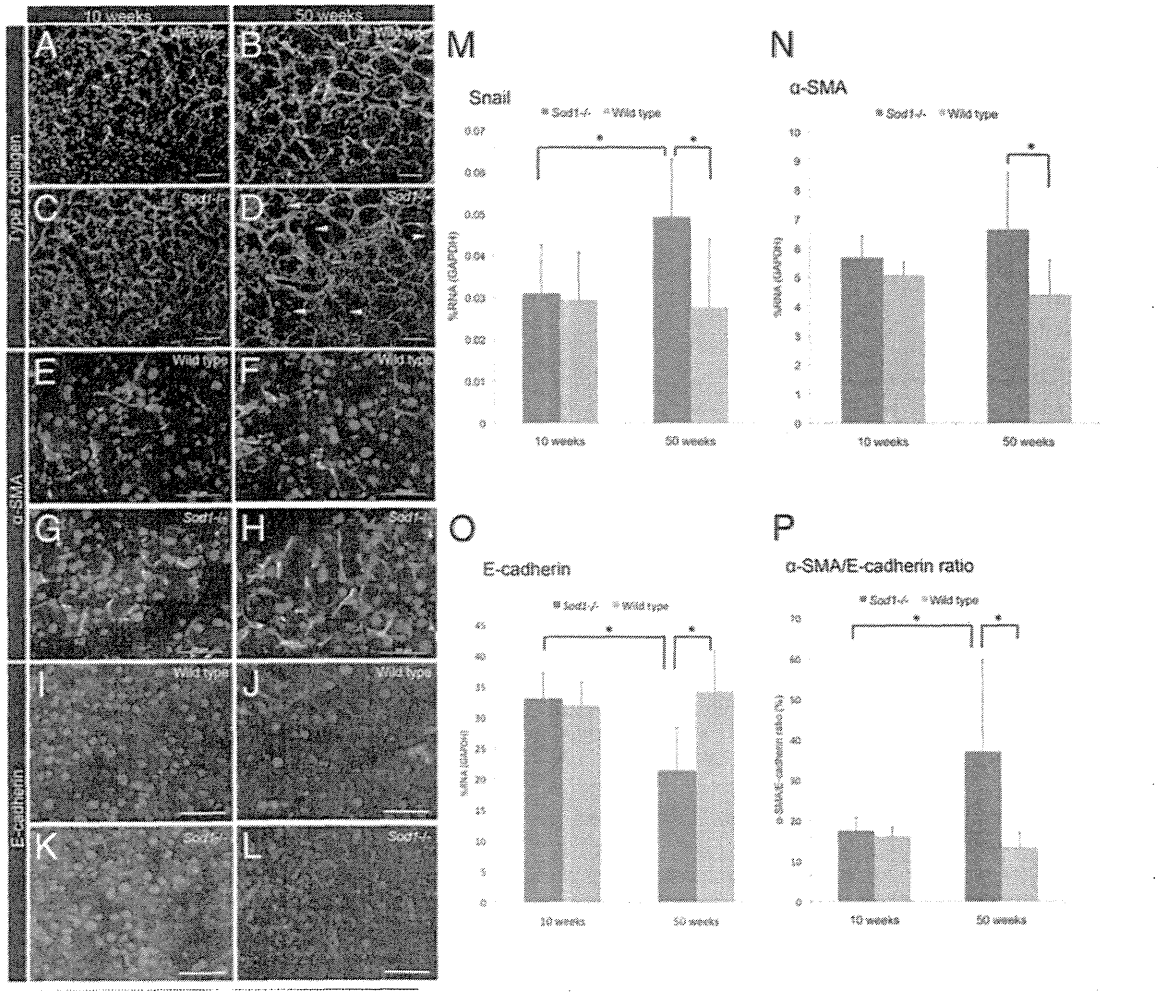

Figure 6. IHC and quantitative transcript evaluation of EMT in the lacrimal gland of WT and *Sod1*$^{-/-}$ mice. IHC using anti–collagen type I antibody (**A–D**) revealed disruption of basement membrane in 50-week-old *Sod1*$^{-/-}$ mice (**D**). **Arrowhead** showed the location of basement membrane disruption (**D**). IHC staining of α-SMA (**E–H**) in 50-week-old *Sod1*$^{-/-}$ mice (**H**) increased compared with 50-week-old WT mice (**F**). On the other hand, IHC staining of E-cadherin (**I–L**) in 50-week-old *Sod1*$^{-/-}$ mice (**L**) decreased compared with 50-week-old WT mice (**J**). **M:** Quantitative real-time PCR revealed that Snail expression in 50-week-old *Sod*$^{-/-}$ mice was higher than 50-week-old WT mice and 10-week-old *Sod1*$^{-/-}$ mice. **N:** α-SMA expression in 50-week-old *Sod1*$^{-/-}$ mice was higher than 50-week-old WT mice. **O:** E-cadherin expression in 50-week-old *Sod*$^{-/-}$ mice was lower than in 50-week-old WT mice, 10-week-old WT mice, and 10-week-old *Sod1*$^{-/-}$ mice. **P:** The α-SMA/E-cadherin ratio in 50-week-old *Sod*$^{-/-}$ mice was higher than in 50-week-old WT mice, 10-week-old *Sod1*$^{-/-}$ mice, and 10-week-old WT mice. $^{*}P < 0.05$.

Ultrastructural Evidence for EMT in the Lacrimal Glands

Electron microscopy observation of lacrimal gland in the 50-week-old *Sod1*$^{-/-}$ mice revealed loss of polarity of acinar epithelial cells, which is feature of EMT (Figure 7). Higher magnification of electron microscopy also revealed the presence of secretory vesicles and microvilli toward the interstitial area with evidence of increased collagen lay-down (Figure 7).

Lacrimal Gland Secretory Functions Decrease Overtime in the Sod1$^{-/-}$ *Mice, Leading to Ocular Surface Disease*

We measured aqueous tear production with the cotton thread test and divided the values by the respective mouse weights at 10 and 50 weeks. Weight-adjusted aqueous tear production measurements were significantly lower in the *Sod1*$^{-/-}$ ($n = 17$) mice compared with the age- and sex-matched WT ($n = 14$) mice at 10 weeks and 50 weeks (10-week-old *Sod1*$^{-/-}$ mice: 0.094 ± 0.077 μL/g; 50-week-old *Sod1*$^{-/-}$ mice: 0.050 ± 0.035 μL/g; 10-week-old WT mice: 0.175 ± 0.112 μL/g; and 50-week-old WT mice: 0.168 ± 0.089 μl/g) as shown in Figure 8A. A significant decrease of tear production from 10 to 50 weeks was also observed in the *Sod1*$^{-/-}$ mice ($P = 0.026$) (Figure 8A). On stimulation with pilocarpine, the tear secretion tended to decrease from 10 to 50 weeks in the *Sod1*$^{-/-}$ mice with a tendency to increase in the WT mice without statistical significance. However, pilocarpine-stimulated tear secretion was significantly lower ($P = 0.0364$) in the *Sod1*$^{-/-}$ mice at 50 weeks (0.034 ± 0.009 μL/g) compared with the WT mice (0.079 ± 0.010